Significant concentrations of nitryl chloride sustained in the morning: Investigations of the causes and impacts on ozone production in a polluted region of northern China

Yee Jun Tham [1], Zhe Wang [1], Qinyi Li [1], Hui Yun [1], Weihao Wang [1], Xinfeng Wang [2], Likun Xue[2], Keding Lu[3], Nan Ma[4], Birger Bohn[5], Xin Li[5], Simonas Kecorius[4] and Johannes Größ[4], Min Shao[3], Alfred Wiedensohler[4], Yuanhang Zhang [3], and Tao Wang[1*].

[1]Department of Civil and Environmental Engineering, The Hong Kong Polytechnic University, Hong Kong, China,
[2]Environment Research Institute, Shandong University, Jinan, Shandong, China,
[3]State Key Joint Laboratory of Environmental Simulation and Pollution Control, College of Environmental Sciences and Engineering, Peking University, Beijing, China,
[4]Leibniz Institute for Tropospheric Research, Permoserstr. 15, 04318 Leipzig, Germany,
[5]Forschungszentrum Jülich, Institut IEK-8: Troposphäre, 52425 Jülich, Germany.

[*]*Correspondence to:* T. Wang (cetwang@polyu.edu.hk)

Abstract. Nitryl chloride ($ClNO_2$) is a dominant source of chlorine radical in polluted environment and can significantly affect the atmospheric oxidative chemistry. However, the abundance of $ClNO_2$ and its exact role are not fully understood under different environmental conditions. During the summer of 2014, we deployed a chemical ionization mass spectrometer to measure $ClNO_2$ and dinitrogen pentoxide (N_2O_5) at a rural site in the polluted North China Plain. Elevated mixing ratios of $ClNO_2$ (>350 pptv) were observed at most of the nights with low levels of N_2O_5 (<200 pptv). The highest $ClNO_2$ mixing ratio of 2070 pptv (1-min average) was observed in a plume from megacity (Tianjin) and was characterized with faster N_2O_5 heterogeneous loss rate and $ClNO_2$ production rate compared to average condition. The abundant $ClNO_2$ concentration kept increasing even after sunrise and reached a peak 4 hours later. Such highly sustained $ClNO_2$ peaks after sunrise are discrepant from the previously observed typical diurnal pattern. Meteorological and chemical analysis show that the sustained $ClNO_2$ morning peaks are caused by significant $ClNO_2$ production in the residual layer at night followed by downward mixing after break-up of the nocturnal inversion layer in the morning. We estimated that ~1.7-4.0 ppbv of $ClNO_2$ would exist in the residual layer in order to maintain the observed morning $ClNO_2$ peaks at the surface site. Observation-based box model analysis show that photolysis of $ClNO_2$ produced chlorine radical with a rate up to 1.12 ppbv h^{-1}, accounting for 10-30% of primary RO_x production in the morning hours. The perturbation in total radical production leads to an increase of integrated daytime net ozone production by 3% (4.3 ppbv) on average, and with a larger increase of 13% (11 ppbv) in megacity outflow that was characterized with higher $ClNO_2$ and relatively lower OVOC to NMHC ratio.

1 Introduction

Nitryl chloride ($ClNO_2$) is a nocturnal reservoir of reactive nitrogen and chlorine radicals (Cl) that play crucial roles in the next day photochemistry (Young et al., 2012; Mielke et al., 2013; Sarwar et al., 2014). Formation of $ClNO_2$ begins with the oxidation of nitrogen dioxide (NO_2) by ozone (O_3) to yield nitrate radical (NO_3) (R1). NO_3 is very susceptible to sunlight and can react rapidly with nitrogen oxide (NO) and volatile organic compounds (VOCs) (R2-4). At nightfall, the NO_3 begins to accumulate and can further react with NO_2 to give N_2O_5 (R5).

$$NO_2 + O_3 \rightarrow NO_3 \tag{R1}$$

$$NO_3 + h\nu \rightarrow 0.9NO_2 + 0.9O + 0.1NO + 0.1O_2 \tag{R2}$$

$$NO_3 + NO \rightarrow 2NO_2 \tag{R3}$$

$$NO_3 + VOC \rightarrow products \tag{R4}$$

$$NO_3 + NO_2 + M \leftrightarrows N_2O_5 + M \tag{R5}$$
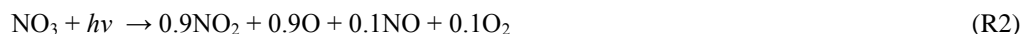
N_2O_5 exist in thermal equilibrium with NO_2 and NO_3, and heterogeneously reacts with chloride containing aerosols (Cl^-) to form $ClNO_2$ and nitrates (NO_3^-) (R6), or undergoes hydrolysis to produce water-soluble nitric acids (HNO_3) (R7) (Finlayson-Pitts et al., 1989).

$$N_2O_5 + Cl^- (aq) \rightarrow ClNO_2 + NO_3^- (aq) \tag{R6}$$

$$N_2O_5 + H_2O (l) \rightarrow 2HNO_3 \tag{R7}$$

The abundance of $ClNO_2$ produced from the heterogeneous uptake of N_2O_5 depends on the availability of Cl^- aerosols and nitrogen oxides ($NO_x = NO + NO_2$) in the atmosphere (Bertram and Thornton, 2009; Brown and Stutz, 2012). Efficient production of $ClNO_2$ was found in the polluted coastal regions that are directly impacted by abundant sea salt aerosol and urban emissions. For instance, Osthoff et al. (2008) measured more than 1 ppbv of $ClNO_2$ in the urban outflows along the coast of Texas; high $ClNO_2$ mixing ratios of up to 3.6 ppbv were detected in the polluted Los Angeles basin (Riedel et al., 2012; Wagner et al., 2012; Mielke et al., 2013). Significant production of $ClNO_2$ was not previously expected in inland regions with limited Cl^- sources until Thornton et al. (2010) found $ClNO_2$ mixing ratio of up to 0.45 ppbv in urban plumes from Boulder, Colorado. This observation suggested the presence of non-oceanic chloride from coal-fired power plants, industries, biomass burning, road salts and soil-dust in inland regions which could support widespread production of $ClNO_2$. Since then, other studies have observed $ClNO_2$ mixing ratios, ranging from tenths of pptv to 1.3 ppbv in polluted inland regions (Mielke et al., 2011; Phillips et al., 2012; Riedel et al., 2013; Faxon et al., 2015).

$ClNO_2$ may subject to some loss processes on water and other surfaces (e.g. Roberts et al., 2008; Kim et al., 2014), but the night-time losses of $ClNO_2$ are expected to be negligible due to its low solubility (Sander, 2015). Its primary sink is

via photolysis during the day, yielding a highly reactive chlorine radical and NO_2 (R8).

$$ClNO_2 + hv \rightarrow Cl + NO_2 \tag{R8}$$
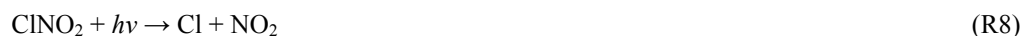
Therefore, $ClNO_2$ typically shows a distinct diurnal pattern where it accumulates at night and decreases gradually to very low levels in the daytime. Under conditions of reduced photolysis, small $ClNO_2$ concentrations may persist during the daytime. For example, Mielke et al., (2013) found that the median lifetime of $ClNO_2$ in respect to photolysis could reach 1.2 h even 4 hours after sunrise at Pasadena (with mixing ratios of $ClNO_2$ of 100 pptv), which was partly caused by the heavy cloud and aerosol cover or fog at the site. More recent measurements at surface sites in London and Houston observed cases with $ClNO_2$ increase after sunrise and peak several hours later with concentration of 40-150 pptv (photolysis lifetime of 2.8-3.5 h) that could result from transport processes of $ClNO_2$ from region with higher $ClNO_2$ concentrations (Bannan et al., 2015; Faxon et al., 2015).

Photolysis of nighttime accumulated $ClNO_2$ during daytime was found to cause rapid production of Cl, with production rate up to 0.03 - 0.50 ppbv h^{-1} (Osthoff et al., 2008; Thornton et al., 2010; Phillips et al., 2012; Riedel et al., 2012, Riedel et al., 2014; Mielke et al., 2015). This Cl precursor was shown to be an important primary radical source as it constituted ~9-13% of the daily primary radical production (Edwards et al., 2013; Young et al., 2014) and exceeded the production of hydroxyl radical (OH) via photolysis of O_3 by up to a factor of 10 for several hours after sunrise (Phillips et al., 2012). Subsequently, the released Cl would oxidize VOCs and enhance ozone production in polluted regions through reactions of R9-R15.

$$Cl + RH \rightarrow R + HCl \tag{R9}$$
$$R + O_2 + M \rightarrow RO_2 + M \tag{R10}$$
$$RO_2 + NO \rightarrow RO + NO_2 \tag{R11}$$
$$RO + O_2 \rightarrow OVOC + HO_2 \tag{R12}$$
$$HO_2 + NO \rightarrow OH + NO_2 \tag{R13}$$
$$NO_2 + hv \rightarrow NO + O(^3P) \tag{R14}$$
$$O(^3P) + O_2 + M \rightarrow O_3 + M \tag{R15}$$
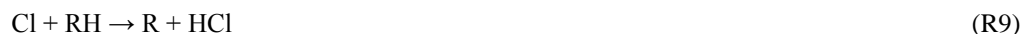
For example, Osthoff et al. (2008) reported an increase of 6 and 9 ppbv of ozone in Houston by constraining 0.65 and 1.5 ppbv of $ClNO_2$ into their model, respectively. Neglecting the contribution of HONO, 1.5 ppbv of $ClNO_2$ could increase ~12 ppbv of ozone in Los Angeles (Riedel et al., 2014). Chemical transport model simulations by Sarwar et al. (2014) suggested that high $ClNO_2$ concentrations in China and Western Europe can lead to daily 8-hour average ozone increase of up to 7 ppbv.

Despite the important role in photochemistry, studies on this Cl precursor in China are sparse. Most of the previously reported studies of $ClNO_2$ were conducted in the US (e.g. Osthoff et al., 2008; Thornton et al., 2010; Riedel et al., 2012; Riedel et al., 2013; Mielke et al., 2013; Faxon et al., 2015), Canada (Mielke et al. 2011, 2015), with a few in Europe (Phillips et al., 2012; Bannan et al., 2015). Recently, measurements of $ClNO_2$ were conducted in Hong Kong, southern China, which observed

high levels of $ClNO_2$ at both surface and mountain sites (Tham et al., 2014; X. Wang et al., 2014; Wang et al., 2016). In a well-processed regional plume, maximum $ClNO_2$ of 4.7 ppbv and N_2O_5 of up to 7.7 ppbv were observed at Mt Tai Mao Shan (957 m a.s.l.), and box model calculations showed significant impacts of the $ClNO_2$ on the next day ozone production, with an increase of ozone of up to 41% (Wang et al., 2016).

The North China Plain (NCP) covers an area of 409,500 km^2 and is home to megacities like Beijing, Tianjin, and Shijiazhuang. It is one of the most polluted regions in China according to the Ministry of Environmental Protection (MEP China, 2015). Due to intense and fast economic development, the emission of NO_x has increased steadily, reaching a peak of 127 Gg N yr^{-1} in 2011 (Mijling et al., 2013). High concentrations of ground-level O_3 were frequently reported in the NCP. For instance, a maximum hourly value of up to 286 ppbv was observed in a rural site north of Beijing (Wang et al., 2006). Ozone over the last two decades has increased at a rate of 2-5% yr^{-1} (Ding et al., 2008; Zhang et al., 2014). The abundant NO_x and O_3 coupled with the large loading of chloride-containing aerosol (Sun et al., 2006; Huang et al., 2014; Sun et al., 2015) may make the heterogeneous uptake and chlorine activation processes particularly important in driving the formation of ozone and secondary aerosol in this region.

In summer 2014, we deployed a chemical ionization mass spectrometer (CIMS) for the first field measurement of $ClNO_2$ in the NCP. It was a part of an international collaborative field campaign, the CARE-Beijing 2014 (Campaigns of Air Quality Research in Beijing and Surrounding Regions) with the major aim to understand the oxidative processes in the region. In the present paper, we give an overview of the measurement results of $ClNO_2$ and its precursors, N_2O_5, and related species. We then examine the factors that affect the $ClNO_2$ production. We also investigate the cause of sustained $ClNO_2$ peaks observed after sunrise and the potential sources of aerosol chloride that drive the $ClNO_2$ productions. The impacts of the $ClNO_2$ on the primary radical productions and ozone formation are then assessed with a measurement-constraint chemical model.

2 Methodology

2.1 Site description

This study took place at a semi-rural site (38.665° N, 115.204° E) in Wangdu County of Hebei province. Figure 1 shows the location of the measurement site in relation to the topography and emission sources in the NCP. Although the site is located in an area with rural/suburban development, it is impacted by anthropogenic emissions. The national capital, Beijing (population > 21 million), is located ~170 km in the northeast, and another megacity, Tianjin (population >15 million) is situated about 180 km to the east, while Shijiazhuang (population >12 million) which is the capital and largest city of Hebei province is 90 km to the southwest. In addition to these megacities, a prefecture-level city, Baoding, is 33 km to the northeast (Fig. 1b). The immediate surrounding area (i.e. within 5 km) of the sampling site is mostly covered by agricultural lands (Fig. 1c). The closest large local emission sources include a national highway and a provincial road, which are about 1-2 km away

from the site. The major town area of Wangdu County is located ~5 km to the northwest while many densely spaced villages are sporadically spread around the area.

Dozens of coal-fired power stations are situated within a radius of 200 km. Among the nearest are Datang power station (capacity 650 MW) which is 27 km in the northeast and Dingzhou power station (capacity 2520 MW) which is 35 km in the southwest. Emission from the agriculture activities also have impacts on the site. The field study is in the harvesting season of winter wheat (Sun et al., 2007) and burning activities were frequently observed in the region, as indicated by the active fire hotspots obtained from FIRMS (MODIS C5, data available at https://earthdata.nasa.gov/firms) (see Fig. S1 in supplementary information (SI)). The less developed area of Taihang Mountains range (main peak = 2,882 m a.s.l) is located at 50-100 km in the north to west sector and the nearest coastline of Bohai Sea is ~200 km in the east.

2.2 Chemical ionization mass spectrometer

$ClNO_2$ and N_2O_5 were concurrently measured with a quadrupole chemical ionization mass spectrometer (THS Instruments, Atlanta). The principle and the calibration of the CIMS have been described in Wang et al. (2016). Briefly, iodide ions (I^-) were used as primary ions and the N_2O_5 and $ClNO_2$ were detected as ion clusters of $I(N_2O_5)^-$ and $I(ClNO_2)^-$ at 235 and 208 m/z, respectively. The CIMS measured N_2O_5 and $ClNO_2$ with a time resolution of ~7s. Data were later converted into 1 min averages for further analysis. During the Wangdu field study, the instrument background was determined by diverting the sampling flow through a filter fully-packed with activated carbons. Off-line calibrations of N_2O_5 and $ClNO_2$ were performed every day on the site, while standard addition of N_2O_5 into the ambient air was performed every 3 hours to monitor the sensitivity changes due to ambient conditions. More details on the calibration procedures can be found elsewhere (Wang et al., 2016). A corona discharge device (THS Instruments) was applied to generate I^- from mixture of CH_3I/N_2 (0.3% v/v) at the beginning of the measurement period (20 June – 26 June 2014) due to delay in shipment of a radioactive source. The large background signals from the corona discharge source (see Fig. S2) gave rise to detection limit of 16 pptv for N_2O_5 and 14 pptv for $ClNO_2$ (3σ, 1 min-averaged data). The corona discharge source was replaced by an alpha radioactive source, ^{210}Po (NRD, P-2031-2000) from 27 June 2014 until the end of the study, which improved the detection limits for the latter period were improved to 7 pptv for N_2O_5 and 6 pptv for $ClNO_2$ (3σ, 1 min-averaged data). The average sensitivity of the system with corona discharge setup was 1.11 ± 0.23 pptv/Hz for N_2O_5 and 1.10 ± 0.11 pptv/Hz for $ClNO_2$, with the average sensitivity of 1.32 ± 0.35 pptv/Hz and 1.40 ± 0.28 pptv/Hz for N_2O_5 and $ClNO_2$, respectively, for radioactive source (see Fig. S3).

The CIMS instrument was housed in a trailer. The sampling line was a 7.5-m long PFA-Teflon tubing (¼" O.D.). The inlet was set at ~2 m above the roof and ~10 m from ground level with a total sampling flow of ~11 standard liters per minute (SLPM). The inlet configuration was similar to a virtual impactor which is intended to remove large particles (e.g. Kercher et al., 2009; Kulkarni et al., 2011). Only ~4 SLPM from the total flow was diverted to the CIMS, ozone and NO_x analyzer while

the rest was dumped. The total residence time in the sampling system was less than a second. In order to minimize the effect of the particles deposited on the surface of the sampling inlet, the orifice, tubing and fittings were replaced and washed with ultrasonic every day (Wang et al., 2016). Examination of the measurement data did not show evidence of conversion of ambient N_2O_5 to $ClNO_2$ in the inlet. For instance, there were occasions when the N_2O_5 signal increased significantly with no

5   enhancement in $ClNO_2$, suggesting that the $ClNO_2$ was not produced in the inlet. Measurement of 208 *m/z* and its isotopic $(I(^{37}ClNO_2)^-)$ was consistent with the natural abundance of chlorine isotopes (refer Fig. S4). The uncertainty of the measurement is estimated to be ±25% with a precision of 3%. The ambient measurements of N_2O_5 and $ClNO_2$ were available from 20 June to 9 July 2014.

10   **2.3 Other measurements**

The measurement techniques for trace gases and aerosols which are used to support the present analysis are summarized in Table 1. During the Wangdu study, most of the trace gases were simultaneously measured by different instruments/techniques. The agreement between these instruments/techniques and justification on the data set selections are discussed in another

15   manuscript (Z. Tan et al., 2016, submitted to this issue of Atmospheric Chemistry and Physics). Briefly, NO and NO_2 were measured by the chemiluminescence/photolytical conversion techniques, while total reactive nitrogen (NO_y) was determined by the chemiluminescence method with a molybdenum oxide (MoO) catalytic converter. O_3 was quantified by a UV absorption analyzer. Sulfur dioxide (SO_2) was measured by a pulsed UV fluorescence analyzer and carbon monoxide (CO) with an infrared photometer. C_2-C_{10} hydrocarbons (NMHCs), formaldehyde (HCHO), and other oxygenated hydrocarbons (OVOCs)

20   were measured with an online gas chromatograph (GC) equipped with a mass spectrometer and a flame ionization detector (FID), a Hantzsch fluorimetric monitor, and proton-transfer-reaction mass spectrometer (PTR-MS), respectively (Yuan et al., 2010, 2012; M. Wang et al., 2014). Methane was measured by cavity ring down spectroscopy technique (CRDs). Measurement of nitrous acid (HONO) was performed by a long-path absorption photometer (LOPAP) instrument (X. Li et al., 2014; Liu et al., 2016).

Particle mass concentrations ($PM_{2.5}$) were measured using a standard Tapered Element Oscillating Microbalances (TEOM). The ionic compositions of $PM_{2.5}$ were determined by a gas aerosol collector (GAC)-ion chromatography system (Dong et al., 2012). The dry-state particle number size distribution was determined by combining the data (Pfeifer et al., 2014) from a Mobility Particle Size Spectrometer (Dual TROPOS-type SMPS; Birmili et al., 1999; Wiedensohler et al., 2012) and

30   an Aerodynamic Particle Size Spectrometer (TSI-type APS model 3321; Pfeifer et al., 2016) covering the size ranges from 4-800 nm (mobility particle diameter) and 0.8-10 µm (aerodynamic particle diameter), respectively. The ambient (wet) particle number size distributions as function of the relative humidity were calculated from a size-resolved kappa-Köhler function determined from real time measurement of a High Humidity Tandem Differential Mobility Analyzer (HHTDMA) (Hennig et

al., 2005; Liu et al., 2014). Ambient particle surface area concentrations (S_a) were calculated based on the (wet) ambient particle number size distribution assuming spherical particles.

Meteorological parameters including wind direction, wind speed, relative humidity (RH), pressure and temperature were measured with an ultrasonic anemometer and a weather station on a 20-m height tower which was situated 30 m from the trailers. Photolysis frequencies were determined from actinic flux densities measured by a spectroradiometer (Meteorologie Consult) (Bohn et al., 2008).

2.4 Meteorological and dispersion models

Weather Research and Forecasting model (WRF) was used for the simulation of meteorological fields during the study. Four nested domains were adopted for WRF simulations, covering whole China, northern China, North China Plain, and the surrounding area of the Wangdu site, with a grid size of 27, 9, 3 and 1 km, respectively. Other settings utilized in this study were the same as those described in Wang et al. (2016). The simulation results from the WRF were validated by using hourly surface observation data obtained from China Meteorological Agency (CMA). WRF simulations generally reproduced the meteorology conditions in NCP during the campaign (refer to Table S1).

With the hourly WRF output, HYbrid Single-Particle Lagrangian Integrated Trajectory model (HYSPLIT) (Draxler et al., 2014) was adopted to investigate the history of air masses that arrived at the measurement site. The HYSPLIT model was run in the dispersion mode for 12 hours backward in time, where 2500 particles were released at the sampling site and the hourly positions of these particles were tracked during this period. More detailed settings and descriptions of the HYSPLIT model can be found in Wang et al. (2016).

2.5 Chemical box model

In order to evaluate the contributions of $ClNO_2$ to daytime primary radical and O_3 production, an explicit observation-based chemical box model was utilized. The model was developed based on the latest version of Master Chemical Mechanism v3.3 (Jenkin et al., 2015) and was updated with a Cl chemistry module including 205 reactions of the inorganic mechanisms of Cl and VOCs degradations initiated by Cl (Xue et al, 2015).

The observation data of $ClNO_2$, HCl, HONO, O_3, NO, NO_2, SO_2, CO, CH_4, C_2-C_{10} NMHCs, OVOCs (methanol, formaldehyde, acetone, acetaldehyde, acetic acid, MEK, MTBE), H_2O, temperature, pressure and aerosol surface area were averaged or interpolated. The model was constrained by the observation data every 10 min. The average concentration for each species and meteorological input are shown in Table S2. The photolysis frequency input of NO_2 (j_{NO2}), HONO (j_{HONO}),

O_3 (j_{O1D}) and $ClNO_2$ (j_{ClNO2}) were determined from the field measurement. The j_{ClNO2} here was determined based on the cross section recommended by Sander et al. (2011). It should be noted that the j_{ClNO2} would be around 20% smaller using the most recent NASA-JPL recommendation based on a work by Ghosh et al. (2012). Photolysis frequency of other related compounds were predicted following the function of solar zenith angle (Saunders et al., 2003) in the model and were scaled according to the field measured j_{NO2}. The lifetime of the unmeasured species with respect to physical first order loss rate was set as 6 h which equals to a deposition velocity of 4.63 cm s^{-1} in a 1000 m deep boundary layer. The model was run for 24-hours period with the starting time set at 00:00 local time and was repeatedly run for 6 times to stabilize the unmeasured intermediate species. The daytime output from the final run was used for further analysis of the primary radical production and O_3 production and loss processes.

3 Results and discussion

3.1 Overview of measurement results

Figure 2 depicts the temporal variations of $ClNO_2$, N_2O_5, related trace gases, $PM_{2.5}$ and selected meteorological parameters for the study period. The data gaps were caused by technical problems, calibrations or maintenance of the instruments which usually took place in the afternoon of each day. Elevated $ClNO_2$ was measured in all of the 13 nights with full CIMS measurements which show typical night-time concentrations larger than 350 pptv. The highest $ClNO_2$ was observed on 20-21 June with maximum mixing ratio of 2070 pptv. There were several nights when $ClNO_2$ mixing ratios were less than 200 pptv (e.g. on 24-25, 28-29 June, and 8-9 July). The observed $ClNO_2$ levels at Wangdu are comparable with previous measurements made in both coastal (e.g. Osthoff et al., 2008; Riedel et al., 2012; Mielke et al., 2013) and inland sites (e.g. Thornton et al., 2010; Phillips et al., 2012; Riedel et al., 2013). As for N_2O_5, low concentrations (<200 pptv) were observed in every night, implying fast loss of N_2O_5, except in the night of 28-29 June when mixing ratio of up to 430 pptv were observed in the air masses with low humidity (RH = ~40%) and NO (<2 ppbv).

The observation of elevated $ClNO_2$ is in-line with the expectation of ubiquitous $ClNO_2$ precursors like NO_x, O_3 and aerosols in the NCP environment. As shown in Figure 2, afternoon mixing ratios of O_3 exceeded 90 ppbv on a majority of days, with a maximum value of 146 ppbv, indicative of intense photochemical reactions during the study period. NO_x mixing ratios were in the range of 10-80 ppbv, which reflects strong emissions of NO_x in the region. Similarly, aerosol loading was quite high, with $PM_{2.5}$ mass concentration larger than 60 µg m^{-3} on most of the days, with the highest value of 220 µg m^{-3}.

Figure 3 shows the 12-h backward particle dispersion trajectories with 08:00 local time (LT) as the starting time during 21 June – 9 July 2014. There were no significant changes in the origins of air masses for those trajectories arriving at 00:00 and 14:00 (Fig. S5 and S6). The study period can be meteorologically separated into three parts. The first part, 21-23 June, indicates air masses from megacities of Beijing and Tianjin (passing over Baoding) in the northeast. The highest $ClNO_2$

level was observed in this period. The second part begins at 24 June and ends 7 July with large majority of air masses originating from the southern sector and passing over a portion of urban areas of Shijiazhuang. The $ClNO_2$ mixing ratios were in the range of tens of pptv to 1.2 ppbv. The final part is 8-9 July with air masses mostly from the less developed mountainous areas in the northwest sector, and the $ClNO_2$ concentrations were low. The entire field campaign was therefore dominated by air masses from southern regions, which is the typical summertime condition in the NCP.

3.2 Diurnal variations

Figure 4a illustrates the mean diurnal variation of $ClNO_2$ and relevant chemical data during the campaign. $ClNO_2$ exhibited a clear diurnal cycle with accumulation of $ClNO_2$ after sunset (~20:00) and reached a peak at ~08:00 in the morning. It then declined gradually to concentrations near the detection limit at noon. The average mixing ratios of $ClNO_2$ were up to 550 pptv. Its precursors, N_2O_5, only showed a small peak right after sunset with maximum average mixing ratio of 80 pptv, and remained at levels near the detection limit of the CIMS for the rest of the night. The NO_y, NO_x and S_a also showed a similar pattern as $ClNO_2$. They increased at sunset with average nighttime concentration of 29 ppbv, 21 ppbv and 1880 μm^2 cm^{-3}, respectively, and were at lowest levels in mid-day. The average night-time NO_x to NO_y ratio was 0.72. Diurnal variation of O_3 was anti-correlated with that for NO_x, with the former concentration rapidly decreasing as night falls.

The highest mixing ratio of $ClNO_2$ was observed on 20-21 June in the outflow of Tianjin megacity (see Fig. 3). We termed it as the megacity case in the remaining of the paper. The $ClNO_2$ mixing ratios in the megacity case were in the range of 110 to 2070 pptv, while N_2O_5 peaked at 170 pptv (Figure 4b). NO_y, O_3 and S_a were generally at similar levels with the average condition, but the NO_x was less abundant at this night compared to the campaign average, with a mean value of 16 ppbv. Smaller NO_x/NO_y ratio of ~0.55 were found on this night, indicating more aged air masses being sampled.

3.3 Factors affecting ClNO₂ production

In this section, we examine the factors that may have caused the large difference of $ClNO_2$ levels in the megacity case and campaign average. Ambient $ClNO_2$ concentrations are affected by several factors including: 1) production rate of NO_3 ($P(NO_3)$); 2) N_2O_5 reactivity (i.e. heterogeneous loss on aerosol surface, homogeneous reaction and dissociation to NO_3); and 3) production yield of $ClNO_2$ (ϕ). The calculated nighttime $P(NO_3)$ through R1, $P(NO_3) = k_{NO2+O3}[NO_2][O_3]$, do not show much difference, with 1.7 ± 0.6 ppbv h^{-1} in campaign average and 1.3 ± 0.5 ppbv h^{-1} in the megacity case.

The N_2O_5 reactivity was assessed with inverse N_2O_5 steady state lifetime analysis by using Eq. (1) and (2) below (e.g. Platt et al., 1984; Brown et al., 2003, 2006, 2009, 2016).

$$\tau(N_2O_5)^{-1} = \frac{P(NO_3)}{[N_2O_5]} = \frac{k(NO_3)}{K_{eq}[NO_2]} + k(N_2O_5)_{het} \qquad \text{(Eq. 1)}$$

$$k(NO_3) = k_{NO+NO3}[NO] + \sum_i k_i [VOC_i] \qquad \text{(Eq. 2)}$$

The steady state inverse lifetimes of N_2O_5, $\tau(N_2O_5)^{-1}$, is the sum of the N_2O_5 loss rate through NO_3 (i.e. $k(NO_3)/K_{eq}[NO_2]$), and N_2O_5 heterogeneous loss rate coefficient ($k(N_2O_5)_{het}$) (see Eq. 1). The total reactivity can be obtained by the ratio of $P(NO_3)$ to the observed N_2O_5 mixing ratios (Brown et al., 2009). K_{eq} is the temperature-dependent equilibrium coefficient in R5, and the $k(NO_3)$ is the loss rate coefficient of NO_3 with NO and VOCs (see Eq. 2). Thus $k(N_2O_5)_{het}$ can be obtained by subtracting $k(NO_3)/K_{eq}[NO_2]$ from the determined $\tau(N_2O_5)^{-1}$. We only conduct analysis for the period between ~20:30 (0.5 h after sunset) until ~23:30 when there were no significant NO plumes (refer Fig. 4), as interception of fresh emissions could lead to the failure of the N_2O_5 steady-state approximation in the air mass (e.g. Brown et al. 2003, 2011, 2016).

Figure 5a shows the averaged total N_2O_5 reactivity and fractions of N_2O_5 loss through NO_3 and heterogeneous loss of N_2O_5 for both campaign average and the megacity case. The determined $\tau(N_2O_5)^{-1}$ is 1.3 x 10^{-2} s^{-1} for campaign average and 5.8 x 10^{-3} s^{-1} for the megacity case, suggesting that the average total loss rate coefficient of N_2O_5 is twice of that of the megacity case. However, the N_2O_5 reactivity is mainly dominated by loss via NO_3 (89%) for the campaign average, which is in-line with its relatively higher VOCs and NO background (Fig. S7). For the megacity case, although it has lower total N_2O_5 reactivity, the $k(N_2O_5)_{het}$ has about equal contribution with the loss via NO_3 and is about a factor of 2.4 faster than the campaign average. This gives a larger N_2O_5 uptake coefficient (γ) of 0.030 in the megacity case compared to 0.014 in the campaign average (which is estimated from Eq. 3, where c_{N2O5} is the mean molecular speed of N_2O_5).

$$k(N_2O_5)_{het} = \frac{1}{4} c_{N2O5} S_a \gamma \qquad \text{(Eq. 3)}$$

The ClNO$_2$ yield that best fits the observations can be estimated by dividing the ClNO$_2$ concentration over the integrated amount of N_2O_5 uptake loss, as shown in Eq. (4).

$$\phi = \frac{[ClNO_2]}{\int k(N_2O_5)_{het}[N_2O_5] \, dt} \qquad \text{(Eq. 4)}$$

Comparable average ClNO$_2$ yield of 0.30 and 0.35 are found in the campaign average and megacity case, respectively.

The ClNO$_2$ production rate depends on the N_2O_5 heterogeneous loss rate coefficient, mixing ratios of N_2O_5 and ϕ, which can be predicted with Eq. (5) when the loss of ClNO$_2$ is negligible during the night-time.

$$\frac{d[ClNO_2]}{dt} = k(N_2O_5)_{het}[N_2O_5]\phi \qquad \text{(Eq. 5)}$$

As illustrated in Fig. 5b, the predicted ClNO$_2$ production rate is a factor of 4 larger than the campaign average. The larger ClNO$_2$ production rate can be justified by the twice higher $k(N_2O_5)_{het}\phi$ and more abundant N_2O_5 (c.a. 2 times larger) in the megacity case that was due to the less N_2O_5 loss through conversion to NO_3 (as shown above). This result is consistent with the observed fourfold higher ClNO$_2$ mixing ratios in the megacity case compared to the average condition (c.f. Fig. 4),

demonstrating that the faster heterogeneous N_2O_5 loss and smaller loss via NO_3 in the megacity case were the major reasons contributing to the larger $ClNO_2$ concentrations.

3.4 Sustained $ClNO_2$ morning peaks

A distinct feature of the $ClNO_2$ is the elevated concentrations sustained after sunrise. Figure 6 depicts the expanded view of the morning $ClNO_2$ peaks together with related chemical characteristics in the campaign average and megacity case. $ClNO_2$ concentration continued to increase after sunrise (at ~04:40) and persisted for 4 hours from sunrise for almost every day. The average mixing ratio of the morning $ClNO_2$ peak was 550 pptv with the megacity case reaching ppbv level. These results are different from the typical diurnal patterns of $ClNO_2$ observed at other places, which usually show a decline of $ClNO_2$ levels at sun rises (e.g. Osthoff et al., 2008; Thornton et al., 2010; Mielke et al., 2013; Tham et al., 2014). As outlined in the introduction, morning peaks of $ClNO_2$ were also observed in London (Bannan et al., 2015) and Texas (Faxon et al., 2015), but they were much smaller than the values at Wangdu.

3.4.1 Causes of $ClNO_2$ morning peaks

The $ClNO_2$ enhancement ($\Delta ClNO_2$) in the morning could be caused by in-situ $ClNO_2$ production and/or downward mixing of the $ClNO_2$ which has been produced in the residual layer (RL) over the night. We calculated the in-situ production of $ClNO_2$ (the area shaded in light grey in the Fig. 6) by using Eq. (6), which is similar to Eq. (3), with additional consideration of $ClNO_2$ loss via photolysis. Since the $k(N_2O_5)_{het}$ and ϕ determined earlier (in section 3.3) are no longer applicable during the daytime, the N_2O_5 heterogeneous loss rate here was estimated from Eq. (7), where γ is the N_2O_5 uptake coefficient and c_{N2O5} is the mean molecular speed of N_2O_5.

$$\frac{d[ClNO_2]}{dt} = k(N_2O_5)_{het}[N_2O_5]\phi - j_{ClNO2}[ClNO_2] \tag{Eq. 6}$$

$$k(N_2O_5)_{het} = \frac{1}{4} c_{N2O5} S_a \gamma \tag{Eq. 7}$$

We used a γ of 0.03 and unity ϕ of 1.0 in the calculations. These numbers are considered as upper end values based on previous field studies (Brown et al., 2006; Bertram et al., 2009; Riedel et al., 2013). As shown in the lower panel of Fig. 6, the calculated $\Delta ClNO_2$ with $\gamma\phi = 0.03$ cannot reproduce the observed increases in $ClNO_2$. Larger $\gamma\phi$ of 0.06 - 0.09 would be needed, but such large uptake coefficients and yields are not supported by the currently available data in the literature. Therefore, we think that in-situ $ClNO_2$ production is not the main reason for the $ClNO_2$ morning peak.

Meteorological and chemical data point to the entrainment of $ClNO_2$ rich air aloft after sun rise as the cause of the $ClNO_2$ morning peaks. Figure 7 shows the fractions of air arriving at the measurements site from various altitudes at different time of day based on the simulations of WRF-HYSPLIT. Vertical mixing was limited prior to sunrise (~04:00) as most of the

air masses were confined to ground level (< 200 m above ground level, a.g.l.). Shortly after sunrise (~05:00), contributions of air masses from the higher levels began to increase after the break-up of nocturnal boundary layer (NBL). As time advanced, larger fraction of higher-level air masses impacted the surface site. Chemical data is consistent with the meteorological analysis. As shown in Fig. 6, the SO_2/NO_y ratios in both cases increased up to 0.6-0.8 after sunrise, indicative of the impact of plumes from coal-fired facilities like power plants. The power-plant plumes from elevated stacks typically reside above the nocturnal boundary layer (NBL) due to poor mixing at night. Coal-fired power plants emit large amount of NO_x and Cl^- containing aerosols, in addition to SO_2 (McCulloch et al., 1999; Zhao et al., 2008). Together with high O_3 produced in the preceding daytime and aerosol loadings, significant production of $ClNO_2$ above the NBL are expected and indeed have been observed in previous field studies (Wagner et al., 2012; Young et al., 2012; Riedel et al., 2013). In the present study, the $ClNO_2$ precursors like Cl^- aerosol and $P(NO_3)$ and a co-product of chlorine activation, nitrate (NO_3^-) aerosol also showed significant enhancement in the early morning hours (see Fig. 6).

3.4.2 Estimation of $ClNO_2$ concentrations in the residual layer

We estimate the amount of the $ClNO_2$ that would exist in the residual layer to maintain the observed $ClNO_2$ at ground level. Here we use a simplified one dimensional (1-D) model to illustrate the mixing process. This model contains two layers of air before sunrise; NBL and RL, with $ClNO_2$ concentrations of C_n and C_r, respectively (see Fig. S8). We assume no mixing of air masses (and $ClNO_2$) between the two layers. After sunrise, the two layers are efficiently mixed, yielding a constant concentration of $ClNO_2$ (C_p). The heights of the daytime planetary boundary layer (PBL) and NBL were calculated by the WRF model, which has been previously demonstrated to be capable of reproducing the PBL heights with a bias of about -13% (Hu et al., 2010). The difference in the heights of PBL and NBL is the depth of the RL. C_n and C_p are the observed mixing ratios before (at 05:00) and after (at 08:00) sunrise, respectively. The concentration in RL layer before sunrise can be estimated by the mass balance approach taking consideration of loss of $ClNO_2$ from photolysis between 05:00 and 08:00 (Eq. (8)).

$$C_p \times H_p = (C_n \exp^{(-j\text{ClNO2}t)} \times H_n) + (C_r \exp^{(-j\text{ClNO2}t)} \times H_r) \qquad \text{(Eq. 8)}$$

Where j_{ClNO2} is photolysis rate of $ClNO_2$ and t is time. The estimated $ClNO_2$ concentration in the RL may subject to underestimation due to the omission of the upward diffusion of $ClNO_2$ in the RL to the free troposphere.

For the campaign average, WRF calculated boundary layer height is 30 m and 325 m (a.g.l.) at 5:00 and 8:00, respectively (refer to Fig. S9). This gives a mixing ratio of $ClNO_2$ in the RL of 1.7 ppbv. For the megacity case with boundary layer height of 72 m at 05:00 and 610 m at 08:00, the $ClNO_2$ in the RL by sunrise would be 4.0 ppbv. The uncertainties of the simulated boundary layer heights may affect the calculated $ClNO_2$ concentration. Recalculation of the $ClNO_2$ concentration by increasing the simulated nocturnal boundary layer height (05:00) by a factor of 2 while remaining the same boundary layer height at 08:00 shows a difference in calculated $ClNO_2$ of less than 10%. These estimated $ClNO_2$ concentrations are within the range of aircraft and tower measurements in RL in the US (Wagner et al., 2012; Young et al., 2012; Riedel et al., 2013)

and are comparable to the highest ClNO$_2$ observed at a mountain site in southern China (Wang et al., 2016). These results suggest that elevated ClNO$_2$ may be frequently present in the residual layer of this region.

3.5 Sources of chloride aerosols

The elevated ClNO$_2$ at Wangdu site requires sufficient amount of chloride aerosols to support its production. Abundant fine Cl$^-$ aerosols was frequently observed during night hours (20:00-09:30) with a mean concentration of 1.6 µg m^{-3} and maximum of 6.8 µg m^{-3} (Fig. 8). The presence of gas-phase HCl during the night (mean = 0.78 ppbv) also can continuously replenish the Cl$^-$ aerosol. The Cl$^-$ concentrations in our study are comparable to those previously observed in the NCP (Sun et al., 2006; Huang et al., 2014; Sun et al., 2015). As can be seen in Figure 3, back-trajectories at Wangdu indicated the air was mainly of continental origins with limited direct influences from the oceans. Chemical data also provide evidence for non-oceanic Cl$^-$ sources. The Cl$^-$ aerosol showed good correlation (r >0.75) with SO$_2$ in 11 out of 16 nights, including 4 nights with concurrent good correlation (r >0.75) with a biomass burning tracer of acetonitrile (CH$_3$CN) (see Table 2). These results suggest that coal-fired power plants are a dominant source of chloride in the region with additional contributions from biomass burning. Significant chlorine content (260 mg kg^{-1}) has been found in the coal used in China (Zhang et al., 2012). Under high temperature and oxygen free conditions, combustion of coal can release up to 97% of the chlorine in the coal in the form of HCl gas (Gibb, 1983) which can then be transformed into aerosol phase (Cl$^-$) through neutralization reactions in the ambient air. The contribution of biomass burning at Wangdu can also be seen in the active fires data on the nights with good correlation between Cl$^-$ aerosol and CH$_3$CN. Figure 9 shows an example of burning activities mostly in south of Wangdu on 28-29 June. Li et al. (2007) measured composition of smoke from burning of wheat straw and maize stover harvested in NCP and found 13.8% and 23.0% of Cl$^-$ in the PM$_{2.5}$ mass loading, respectively. Recent field measurement of biomass burning plumes during the harvesting period in China also indicated a drastic increase in the Cl$^-$ concentration (>20 µg m^{-3}) (J. F. Li et al., 2014).

3.6 The impact of ClNO$_2$ on primary radical and ozone production

This section examines the contributions of ClNO$_2$ to the primary RO$_x$ (OH+HO$_2$+RO$_2$) radical and in-situ ozone production at Wangdu using the observation-constrained box model described in Section 2.5. The analysis focuses on campaign average condition and the megacity case. The mean concentrations of trace gases and other parameters that serve as inputs are shown in Table S2.

Figure 10a illustrates the Cl production rate derived from the photolysis of ClNO$_2$ and without ClNO$_2$ (only from photolysis of Cl$_2$ and HCl+OH). It shows that photolysis of ClNO$_2$ was the predominant source of Cl in Wangdu compared to the reaction of HCl and OH and photolysis of Cl$_2$. The production of Cl was efficient in the morning (from sunrise to ~11:00) and reached maximum at ~08:00 corresponding to the peak concentration of ClNO$_2$. The Cl production rate was up to 0.24

ppbv h^{-1} for average condition, and up to 1.12 ppbv h^{-1} for the megacity case. Figure 10b depicts the primary daytime RO_x production ($P(RO_x)$) from sources including photolysis of $ClNO_2$, OVOCs (excluded HCHO), HCHO, HONO and O_3 (O^1D+H_2O), O_3+VOCs, and NO_3 oxidation. Similar to previous studies, the primary daytime $P(RO_x)$ is dominated by sources from photolysis of HCHO, OVOCs and HONO (Kanaya et al., 2009; Liu et al., 2012; Lu et al., 2013). The photolysis of $ClNO_2$ is particularly important during the morning hours. During 08:00 - 08:30, photolysis of $ClNO_2$ contributed to 10% of the $P(RO_x)$ on average condition and with a much larger contribution of 30% in the megacity case. These results highlight the importance of $ClNO_2$ as a significant source of RO_x radicals in this region. Reader is referred to Z. Tan et al., (2016, submitted to this issue of Atmospheric Chemistry and Physics) for more extensive analysis on the RO_x chemistry at Wangdu.

The effect of $ClNO_2$ photolysis on in-situ ozone production is also relevant. Figure 11 shows the net ozone production rates ($P(O_3)$) during daytime (from 05:00 to 18:00) and the difference in integrated total ozone production simulated with $ClNO_2$ and without $ClNO_2$ input. The O_3 production rates were enhanced throughout the day due to the $ClNO_2$ effect, especially during the morning hours. The increase in net $P(O_3)$ for campaign average reached 0.9 ppbv h^{-1} or 17% during the morning. For the megacity outflow, much higher increases in $P(O_3)$ can be seen in the entire morning, with a maximum of 3.3 ppbv h^{-1} (or 76% increase) at ~08:00. Integrating over the entire daytime period, the increase in total ozone production was 4.3 ppbv (3%) and 11 ppbv (13%) for average condition and the megacity case, respectively. Although not directly comparable, these values are generally within the range of net ozone production increase caused by $ClNO_2$ in previous studies in Houston (Osthoff et al., 2008), Los Angeles (Riedel et al., 2014), and southern China (Xue et al., 2015; Wang et al., 2016).

We notice a large difference in the impact of $ClNO_2$ on ozone production between campaign average and the megacity case. This can be explained by their different $ClNO_2$ and VOCs characteristics. First, for campaign average, the $ClNO_2$ mixing ratio was much lower than that of the megacity case (see section 3.3). The smaller $ClNO_2$ concentrations, in turn, would produce less chlorine radical in the daytime, reducing the production of RO_x which ultimately decreases the O_3 production. A simulation test by only reducing the $ClNO_2$ mixing ratios in the megacity case by a factor of 2.8 (that is, to the same levels of campaign average) showed a sharp drop in the increase of the ozone production from 13% to 6% (Fig. S10a), confirming the importance of $ClNO_2$ mixing ratios in driving the ozone enhancement. Second, the higher OVOC to NMHC fraction in campaign average (see Fig. S11 for the VOCs mix) provided a larger pool of RO_x, and the radical propagation would amplify the OH through efficient radical recycling (Liu et al., 2012), dampening the effect of chlorine radical. Another test by only increasing the $ClNO_2$ mixing ratios in campaign average condition to the same value of the megacity case indicated a relatively smaller increase in the ozone production (9%) (see Fig. S10b) compared to the increased percentage of O_3 production in the megacity case (13%).

The much higher OVOCs mixing ratios to NMHCs in campaign average are likely influenced by the biomass burning activities which are more intense in the regions south of Wangdu (refer to Fig. S1) and the biomass burning-influenced plumes

can be transported to Wangdu by prevailing southerly winds as shown by the trajectories (Fig. 3). During our field measurement, we indeed observed significant increase (up to 170 ppbv) of OVOCs in a fresh biomass burning plume at the midnight of 15 June 2014 (Fig. S12). High content of OVOCs from biomass burning has been previously reported at a mountain–site of the NCP (Inomata et al., 2010). Significant emissions of OVOCs from the burning of Chinese crop residues were also reported in a recent laboratory study (Inomata et al., 2015).

We hence conclude that higher concentrations of $ClNO_2$ and lesser abundant of VOCs (i.e. smaller OVOC to NMHC fraction) in the megacity case resulted in a relatively higher impact of Cl chemistry on the ozone formation. Although we only measured very high $ClNO_2$ concentration in one event of megacity outflow, similar cases occurred in the beginning of the study period during which NO_x, NO_y, S_a and VOCs data were available (but not $ClNO_2$). An examination of the VOCs mix and other chemical compounds confirmed the less abundance of OVOCs but has similar chemical characteristics in these cases (see Fig. S13 for an example of chemical characteristics on 23 and 27 June 2014). Previous studies have shown less abundance of OVOCs relative to NMHCs in and downwind of urban Beijing (Liu et al., 2009; Xu et al., 2011). Thus, we suggest that the effect of $ClNO_2$ on ozone enhancement may be more important in air masses dominated by urban/power plants emissions than those by biomass burning.

4. Summary and conclusions

This first $ClNO_2$ measurement in northern China unambiguously documented the presence of elevated $ClNO_2$ in this highly polluted region. Highest $ClNO_2$ mixing ratio (2070 pptv, 1 min average) was observed in an urban outflow plume on 20-21 June 2014. The air mass was characterized by faster (by a factor of 2.4) N_2O_5 heterogeneous loss as well as larger $ClNO_2$ production rate (by a factor of 4) compared to campaign average condition. The peak concentrations of $ClNO_2$ often occurred 4 hours after sun rise. Downward mixing of $ClNO_2$ rich air in the residual layer is believed to be the cause of these morning peaks, and the mixing ratios of $ClNO_2$ in residual layer are estimated in the range of 1.7-4.0 ppbv. These values are supported by our mountain-top measurement of $ClNO_2$ in Hong Kong with mixing ratio of up to 4.7 ppbv in well processed urban/industrial plumes (Wang et al., 2016). The Wangdu result implies strong productions of $ClNO_2$ in the residual layers over the polluted regions of northern China. We also observed evidence for existence of fine aerosol chloride from non-oceanic sources like coal-fired power plants and burning of crop residues, suggesting the widespread effects of $ClNO_2$ on the oxidative capacity and production of secondary pollutants in this region. Our model calculations suggest a larger impact of $ClNO_2$ on primary radical productions and ozone enhancement in urban/power plant emission dominated air masses compared to biomass burning due to higher levels of VOCs (also larger OVOC to NMHC ratios) and relatively lower $ClNO_2$ in the latter case. More studies in non-biomass burning seasons and in areas adjacent to megacities/power plants are needed to examine the production of $ClNO_2$ and its effect on regional photochemistry. Vertical profile measurements of $ClNO_2$ and related species would be highly desirable.

Acknowledgement. The authors thank Steven Poon, Zha QiaoZhi, Xu Zheng and Wang Hao for the logistics support, to Zhang Li, Liu Xiaoxi, and Steve Sjostedt for help in the modeling and instrumentations, to the CARE-Beijing 2014 team for their contributions in obtaining the data during field campaign. We are grateful to China Meteorological Agency for providing observational meteorological data and to NOAA Air Resources Laboratory for providing the HYSPLIT model. This work was funded by the National Natural Science Foundation of China (41275123 and 91544213) and PolyU Project of Strategic Importance (1-ZE13). The Peking University team acknowledges support from National Natural Science Foundation of China (21190052) and Strategic Priority Research Program of the Chinese Academy of Sciences (XDB05010500). The Leibniz Institute for Tropospheric Research team acknowledge financial funding by Sino German Science Center (No. GZ663).

Reference

Bannan, T. J., Booth, A. M., Bacak, A., Muller, J. B. A., Leather, K. E., Le Breton, M., Jones, B., Young, D., Coe, H., Allan, J., Visser, S., Slowik, J. G., Furger, M., Prevot, A. S. H., Lee, J., Dunmore, R. E., Hopkins, J. R., Hamilton, J. F., Lewis, A. C., Whalley, L. K., Sharp, T., Stone, D., Heard, D. E., Fleming, Z. L., Leigh, R., Shallcross, D. E., and Percival, C. J.: The first UK measurements of nitryl chloride using a chemical ionization mass spectrometer in central London in the summer of 2012, and an investigation of the role of Cl atom oxidation, J. Geophys. Res.-Atmos., 120, 5638-5657, 10.1002/2014JD022629, 2015.

Bertram, T. H., and Thornton, J. A.: Toward a general parameterization of N_2O_5 reactivity on aqueous particles: the competing effects of particle liquid water, nitrate and chloride, Atmos. Chem. Phys., 9, 8351-8363, 10.5194/acp-9-8351-2009, 2009.

Bertram, T. H., Thornton, J. A., Riedel, T. P., Middlebrook, A. M., Bahreini, R., Bates, T. S., Quinn, P. K., and Coffman, D. J.: Direct observations of N_2O_5 reactivity on ambient aerosol particles, Geophys. Res. Lett., 36, L19803, 10.1029/2009gl040248, 2009.

Birmili, W., Stratmann, F., and Wiedensohler, A.: Design of a DMA-based size spectrometer for a large particle size range and stable operation, J. Aerosol Sci., 30, 549-553, 10.1016/S0021-8502(98)00047-0, 1999.

Bohn, B., Corlett, G. K., Gillmann, M., Sanghavi, S., Stange, G., Tensing, E., Vrekoussis, M., Bloss, W. J., Clapp, L. J., Kortner, M., Dorn, H. P., Monks, P. S., Platt, U., Plass-Dulmer, C., Mihalopoulos, N., Heard, D. E., Clemitshaw, K. C., Meixner, F. X., Prevot, A. S. H., and Schmitt, R.: Photolysis frequency measurement techniques: results of a comparison within the ACCENT project, Atmos. Chem. Phys., 8, 5373-5391, 2008.

Brown, S. S., and Stutz, J.: Nighttime radical observations and chemistry, Chem. Soc. Rev., 41, 6405-6447, 10.1039/c2cs35181a, 2012.

Brown, S. S., Dube, W. P., Fuchs, H., Ryerson, T. B., Wollny, A. G., Brock, C. A., Bahreini, R., Middlebrook, A. M., Neuman, J. A., Atlas, E., Roberts, J. M., Osthoff, H. D., Trainer, M., Fehsenfeld, F. C., and Ravishankara, A. R.: Reactive uptake coefficients for N_2O_5 determined from aircraft measurements during the Second Texas Air Quality Study: Comparison to current model parameterizations, J. Geophys. Res.-Atmos., 114, D00F10, 10.1029/2008jd011679, 2009.

Brown, S. S., Dube, W. P., Peischl, J., Ryerson, T. B., Atlas, E., Warneke, C., de Gouw, J. A., Hekkert, S. T., Brock, C. A., Flocke, F., Trainer, M., Parrish, D. D., Feshenfeld, F. C., and Ravishankara, A. R.: Budgets for nocturnal VOC oxidation by nitrate radicals aloft during the 2006 Texas Air Quality Study, J. Geophys. Res.-Atmos., 116, 10.1029/2011jd016544, 2011.

Brown, S. S., Dube, W. P., Tham, Y. J., Zha, Q. Z., Xue, L. K., Poon, S., Wang, Z., Blake, D. R., Tsui, W., Parrish, D. D., and Wang, T.: Nighttime chemistry at a high altitude site above Hong Kong, J. Geophys. Res.-Atmos., 121, 2457-2475, 10.1002/2015JD024566, 2016.

Brown, S. S., Ryerson, T. B., Wollny, A. G., Brock, C. A., Peltier, R., Sullivan, A. P., Weber, R. J., Dube, W. P., Trainer, M., Meagher, J. F., Fehsenfeld, F. C., and Ravishankara, A. R.: Variability in nocturnal nitrogen oxide processing and its role in regional air quality, Science, 311, 67-70, 10.1126/science.1120120, 2006.

Brown, S. S., Stark, H., and Ravishankara, A. R.: Applicability of the steady state approximation to the interpretation of atmospheric observations of NO_3 and N_2O_5, J. Geophys. Res.-Atmos., 108, 10.1029/2003jd003407, 2003.

Ding, A. J., Wang, T., Thouret, V., Cammas, J. P., and Nédélec, P.: Tropospheric ozone climatology over Beijing: analysis of aircraft data from the MOZAIC program, Atmos. Chem. Phys., 8, 1-13, 10.5194/acp-8-1-2008, 2008.

Dong, H. B., Zeng, L. M., Hu, M., Wu, Y. S., Zhang, Y. H., Slanina, J., Zheng, M., Wang, Z. F., and Jansen, R.: Technical Note: The application of an improved gas and aerosol collector for ambient air pollutants in China, Atmos. Chem. Phys., 12, 10519-10533, 10.5194/acp-12-10519-2012, 2012.

Draxler, R., B. Stunder, G. Rolph, A. Stein, and A. Taylor: HYSPLIT_4 User's Guide, NOAA Air Resources Laboratory, Silver Spring, Md., 2014.

Edwards, P. M., Young, C. J., Aikin, K., deGouw, J., Dube, W. P., Geiger, F., Gilman, J., Helmig, D., Holloway, J. S., Kercher, J., Lerner, B., Martin, R., McLaren, R., Parrish, D. D., Peischl, J., Roberts, J. M., Ryerson, T. B., Thornton, J., Warneke, C., Williams, E. J., and Brown, S. S.: Ozone photochemistry in an oil and natural gas extraction region during winter: simulations of a snow-free season in the Uintah Basin, Utah, Atmos. Chem. Phys., 13, 8955-8971, 10.5194/acp-13-8955-2013, 2013.

Faxon, C. B., Bean, J. K., and Ruiz, L. H.: Inland Concentrations of Cl_2 and $ClNO_2$ in Southeast Texas suggest chlorine chemistry significantly contributes to atmospheric reactivity, Atmosphere, 6, 1487-1506, 2015.

Finlayson-Pitts, B. J., Ezell, M. J., and Pitts, J. N.: Formation of chemically active chlorine compounds by reactions of atmospheric NaCl particles with gaseous N_2O_5 and $ClONO_2$, Nature, 337, 241-244, 10.1038/337241a0, 1989.

Ghosh, B., Papanastasiou, D. K., Talukdar, R. K., Roberts, J. M., and Burkholder, J. B.: Nitryl chloride ($ClNO_2$): UV/vis absorption spectrum between 210 and 296 K and $O(^3P)$ quantum yield at 193 and 248 nm, J. Phys. Chem. A, 116, 5796-5805, 10.1021/jp207389y, 2012.

Gibb W.H.: Corrosion resistant materials for coal conversion systems, Meadowcroft, D.B. and Manning, M.I., Applied science, London, p. 25, 1983.

Hennig, T., Massling, A., Brechtel, F. J., and Wiedensohler, A.: A tandem DMA for highly temperature-stabilized hygroscopic particle growth measurements between 90% and 98% relative humidity, J. Aerosol Sci., 36, 1210-1223, 10.1016/j.jaerosci.2005.01.005, 2005.

Hu, X. M., Nielsen-Gammon, J. W., and Zhang, F. Q.: Evaluation of three planetary boundary layer schemes in the WRF Model, J. Appl. Meteorol. Clim., 49, 1831-1844, 10.1175/2010JAMC2432.1, 2010.

Huang, R. J., Zhang, Y., Bozzetti, C., Ho, K. F., Cao, J. J., Han, Y., Daellenbach, K. R., Slowik, J. G., Platt, S. M., Canonaco, F., Zotter, P., Wolf, R., Pieber, S. M., Bruns, E. A., Crippa, M., Ciarelli, G., Piazzalunga, A., Schwikowski, M., Abbaszade, G., Schnelle-Kreis, J., Zimmermann, R., An, Z., Szidat, S., Baltensperger, U., El Haddad, I., and Prevot, A. S.: High secondary aerosol contribution to particulate pollution during haze events in China, Nature, 514, 218-222, 10.1038/nature13774, 2014.

Inomata, S., Tanimoto, H., Kato, S., Suthawaree, J., Kanaya, Y., Pochanart, P., Liu, Y., and Wang, Z.: PTR-MS measurements of non-methane volatile organic compounds during an intensive field campaign at the summit of Mount Tai, China, in June 2006, Atmos. Chem. Phys., 10, 7085-7099, 10.5194/acp-10-7085-2010, 2010.

Inomata, S., Tanimoto, H., Pan, X. L., Taketani, F., Komazaki, Y., Miyakawa, T., Kanaya, Y., and Wang, Z. F.: Laboratory measurements of emission factors of nonmethane volatile organic compounds from burning of Chinese crop residues, J. Geophys. Res.-Atmos., 120, 5237-5252, 10.1002/2014JD022761, 2015.

Jenkin, M. E., Young, J. C., and Rickard, A. R.: The MCM v3.3.1 degradation scheme for isoprene, Atmos. Chem. Phys., 15, 11433-11459, 10.5194/acp-15-11433-2015, 2015.

Kanaya, Y., Pochanart, P., Liu, Y., Li, J., Tanimoto, H., Kato, S., Suthawaree, J., Inomata, S., Taketani, F., Okuzawa, K., Kawamura, K., Akimoto, H., and Wang, Z. F.: Rates and regimes of photochemical ozone production over Central East China in June 2006: a box model analysis using comprehensive measurements of ozone precursors, Atmos. Chem. Phys., 9, 7711-7723, 10.5194/acp-9-7711-2009, 2009.

Kercher, J. P., Riedel, T. P., and Thornton, J. A.: Chlorine activation by N_2O_5: simultaneous, in situ detection of $ClNO_2$ and N_2O_5 by chemical ionization mass spectrometry, Atmos. Meas. Tech., 2, 193-204, 10.5194/amt-2-193-2009, 2009.

Kim, M. J., Farmer, D. K., and Bertram, T. H.: A controlling role for the air-sea interface in the chemical processing of reactive nitrogen in the coastal marine boundary layer, Proc. Natl. Acad. Sci., 111, 3943-3948, 10.1073/pnas.1318694111, 2014.

Kulkarni, P., Baron, P. A., and Willeke, K.: Aerosol Measurement: Principles, Techniques, and Applications, Wiley, 2011.

Li, J. F., Song, Y., Mao, Y., Mao, Z. C., Wu, Y. S., Li, M. M., Huang, X., He, Q. C., and Hu, M.: Chemical characteristics and source apportionment of $PM_{2.5}$ during the harvest season in eastern China's agricultural regions, Atmospheric Environment, 92, 442-448, 10.1016/j.atmosenv.2014.04.058, 2014.

Li, X., Rohrer, F., Hofzumahaus, A., Brauers, T., Haseler, R., Bohn, B., Broch, S., Fuchs, H., Gomm, S., Holland, F., Jager, J., Kaiser, J., Keutsch, F. N., Lohse, I., Lu, K., Tillmann, R., Wegener, R., Wolfe, G. M., Mentel, T. F., Kiendler-Scharr, A., and Wahner, A.: Missing gas-phase source of HONO inferred from Zeppelin measurements in the troposphere, Science, 344, 292-296, 10.1126/science.1248999, 2014.

Li, X., Wang, S., Duan, L., Hao, J., Li, C., Chen, Y., and Yang, L.: Particulate and trace gas emissions from open burning of wheat straw and corn stover in China, Environ. Sci. Technol., 41, 6052-6058, 10.1021/es0705137, 2007.

Liu, H. J., Zhao, C. S., Nekat, B., Ma, N., Wiedensohler, A., van Pinxteren, D., Spindler, G., Muller, K., and Herrmann, H.: Aerosol hygroscopicity derived from size-segregated chemical composition and its parameterization in the North China Plain, Atmos. Chem. Phys., 14, 2525-2539, 10.5194/acp-14-2525-2014, 2014.

Liu, Y., Lu, K., Dong, H., Li, X., Cheng, P., Zou, Q., Wu, Y., Liu, X., and Zhang, Y.: In situ monitoring of atmospheric nitrous acid based on multi-pumping flow system and liquid waveguide capillary cell, J. Environ. Sci. (China), 43, 273-284, 10.1016/j.jes.2015.11.034, 2016.

Liu, Y., Shao, M., Kuster, W. C., Goldan, P. D., Li, X., Lu, S., and de Gouw, J. A.: Source identification of reactive hydrocarbons and oxygenated VOCs in the summertime in Beijing, Environ. Sci. Technol., 43, 75-81, 10.1021/es801716n, 2009.

Liu, Z., Wang, Y., Gu, D., Zhao, C., Huey, L. G., Stickel, R., Liao, J., Shao, M., Zhu, T., Zeng, L., Amoroso, A., Costabile, F., Chang, C. C., and Liu, S. C.: Summertime photochemistry during CAREBeijing-2007: RO_x budgets and O_3 formation, Atmos. Chem. Phys., 12, 7737-7752, 10.5194/acp-12-7737-2012, 2012.

Lu, K. D., Hofzumahaus, A., Holland, F., Bohn, B., Brauers, T., Fuchs, H., Hu, M., Häseler, R., Kita, K., Kondo, Y., Li, X., Lou, S. R., Oebel, A., Shao, M., Zeng, L. M., Wahner, A., Zhu, T., Zhang, Y. H., and Rohrer, F.: Missing OH source in a suburban environment near Beijing: observed and modelled OH and HO_2 concentrations in summer 2006, Atmos. Chem. Phys., 13, 1057-1080, 10.5194/acp-13-1057-2013, 2013.

McCulloch, A., Aucott, M. L., Benkovitz, C. M., Graedel, T. E., Kleiman, G., Midgley, P. M., and Li, Y. F.: Global emissions of hydrogen chloride and chloromethane from coal combustion, incineration and industrial activities: Reactive Chlorine Emissions Inventory, J. Geophys. Res.-Atmos., 104, 8391-8403, 10.1029/1999jd900025, 1999.

Mielke, L. H., Furgeson, A., and Osthoff, H. D.: Observation of $ClNO_2$ in a mid-continental urban environment, Environ. Sci. Technol., 45, 8889-8896, 10.1021/es201955u, 2011.

Mielke, L. H., Furgeson, A., Odame-Ankrah, C. A., and Osthoff, H. D.: Ubiquity of $ClNO_2$ in the urban boundary layer of Calgary, AB, Canada, Canadian J. Chem., 2015.

Mielke, L. H., Stutz, J., Tsai, C., Hurlock, S. C., Roberts, J. M., Veres, P. R., Froyd, K. D., Hayes, P. L., Cubison, M. J., Jimenez, J. L., Washenfelder, R. A., Young, C. J., Gilman, J. B., de Gouw, J. A., Flynn, J. H., Grossberg, N., Lefer, B. L., Liu, J., Weber, R. J., and Osthoff, H. D.: Heterogeneous formation of nitryl chloride and its role as a nocturnal NOx reservoir species during CalNex-LA 2010, J. Geophys. Res.-Atmos., 118, 10638-10652, 10.1002/jgrd.50783, 2013.

Mijling, B., van der A, R. J., and Zhang, Q.: Regional nitrogen oxides emission trends in East Asia observed from space, Atmos. Chem. Phys., 13, 12003-12012, 10.5194/acp-13-12003-2013, 2013.

Ministry of Environmental Protection China: Heavy air pollution lingers in some cities in Beijing-Tianjin-Hebei region and surrounding area, 2015, http://english.mep.gov.cn/News_service/infocus/201512/t20151203_318373.htm.

Osthoff, H. D., Roberts, J. M., Ravishankara, A. R., Williams, E. J., Lerner, B. M., Sommariva, R., Bates, T. S., Coffman, D., Quinn, P. K., Dibb, J. E., Stark, H., Burkholder, J. B., Talukdar, R. K., Meagher, J., Fehsenfeld, F. C., and Brown, S. S.: High levels of nitryl chloride in the polluted subtropical marine boundary layer, Nat. Geosci., 1, 324-328, 10.1038/ngeo177, 2008.

5   Pfeifer, S., Birmili, W., Schladitz, A., Muller, T., Nowak, A., and Wiedensohler, A.: A fast and easy-to-implement inversion algorithm for mobility particle size spectrometers considering particle number size distribution information outside of the detection range, Atmos. Meas. Tech., 7, 95-105, 10.5194/amt-7-95-2014, 2014.

Pfeifer, S., Muller, T., Weinhold, K., Zikova, N., dos Santos, S. M., Marinoni, A., Bischof, O. F., Kykal, C., Ries, L., Meinhardt, F., Aalto, P., Mihalopoulos, N., and Wiedensohler, A.: Intercomparison of 15 aerodynamic particle size 10   spectrometers (APS 3321): uncertainties in particle sizing and number size distribution, Atmos. Meas. Tech., 9, 1545-1551, 10.5194/amt-9-1545-2016, 2016.

Phillips, G. J., Tang, M. J., Thieser, J., Brickwedde, B., Schuster, G., Bohn, B., Lelieveld, J., and Crowley, J. N.: Significant concentrations of nitryl chloride observed in rural continental Europe associated with the influence of sea salt chloride and anthropogenic emissions, Geophys. Res. Lett., 39, L10811, 10.1029/2012gl051912, 2012.

15   Platt, U. F., Winer, A. M., Biermann, H. W., Atkinson, R., and Pitts, J. N.: Measurement of nitrate radical concentrations in continental air, Environ. Sci. Technol., 18, 365-369, 10.1021/es00123a015, 1984.

Riedel, T. P., Bertram, T. H., Crisp, T. A., Williams, E. J., Lerner, B. M., Vlasenko, A., Li, S. M., Gilman, J., de Gouw, J., Bon, D. M., Wagner, N. L., Brown, S. S., and Thornton, J. A.: Nitryl chloride and molecular chlorine in the coastal marine boundary layer, Environ. Sci. Technol., 46, 10463-10470, 10.1021/es204632r, 2012.

20   Riedel, T. P., Wagner, N. L., Dube, W. P., Middlebrook, A. M., Young, C. J., Ozturk, F., Bahreini, R., VandenBoer, T. C., Wolfe, D. E., Williams, E. J., Roberts, J. M., Brown, S. S., and Thornton, J. A.: Chlorine activation within urban or power plant plumes: Vertically resolved $ClNO_2$ and Cl_2 measurements from a tall tower in a polluted continental setting, J. Geophys. Res.-Atmos., 118, 8702-8715, 10.1002/jgrd.50637, 2013.

Riedel, T. P., Wolfe, G. M., Danas, K. T., Gilman, J. B., Kuster, W. C., Bon, D. M., Vlasenko, A., Li, S. M., Williams, E. J., 25   Lerner, B. M., Veres, P. R., Roberts, J. M., Holloway, J. S., Lefer, B., Brown, S. S., and Thornton, J. A.: An MCM modeling study of nitryl chloride ($ClNO_2$) impacts on oxidation, ozone production and nitrogen oxide partitioning in polluted continental outflow, Atmos. Chem. Phys., 14, 3789-3800, 10.5194/acp-14-3789-2014, 2014.

Roberts, J. M., Osthoff, H. D., Brown, S. S., and Ravishankara, A. R.: N_2O_5 oxidizes chloride to Cl_2 in acidic atmospheric aerosol, Science, 321, 1059, 10.1126/science.1158777, 2008.

30   Roberts, J. M., Osthoff, H. D., Brown, S. S., Ravishankara, A. R., Coffman, D., Quinn, P., and Bates, T.: Laboratory studies of products of N_2O_5 uptake on Cl^- containing substrates, Geophys. Res. Lett., 36, L20808, 10.1029/2009gl040448, 2009.

Sander, R.: Compilation of Henry's law constants (version 4.0) for water as solvent, Atmos. Chem. Phys., 15, 4399-4981, 10.5194/acp-15-4399-2015, 2015.

Sander, S. P., Abbatt, J., Barker, J. R., Burkholder, J. B., Friedl, R. R., Golden, D. M., Huie, R. E., Kolb, C. E., Kurylo, M. J., Moortgat, G. K., Orkin V. L., and Wine, P. H.: Chemical kinetics and photochemical data for use in atmospheric studies, Evaluation No. 17, JPL Publication 10-6, Jet Propulsion Laboratory, Pasadena, 2011 (http://jpldataeval.jpl.nasa.gov).

Sarwar, G., Simon, H., Xing, J., and Mathur, R.: Importance of tropospheric $ClNO_2$ chemistry across the Northern Hemisphere, Geophys. Res. Lett., 41, 4050-4058, 10.1002/2014GL059962, 2014.

Saunders, S. M., Jenkin, M. E., Derwent, R. G., and Pilling, M. J.: Protocol for the development of the Master Chemical Mechanism, MCM v3 (Part A): tropospheric degradation of non-aromatic volatile organic compounds, Atmos. Chem. Phys., 3, 161-180, 10.5194/acp-3-161-2003, 2003.

Sun, H. Y., Zhang, X. Y., Chen, S. Y., Pei, D., and Liu, C. M.: Effects of harvest and sowing time on the performance of the rotation of winter wheat-summer maize in the North China Plain, Ind. Crop Prod., 25, 239-247, 10.1016/j.indcrop.2006.12.003, 2007.

Sun, Y. L., Wang, Z. F., Du, W., Zhang, Q., Wang, Q. Q., Fu, P. Q., Pan, X. L., Li, J., Jayne, J., and Worsnop, D. R.: Long-term real-time measurements of aerosol particle composition in Beijing, China: seasonal variations, meteorological effects, and source analysis, Atmos. Chem. Phys., 15, 10149-10165, 10.5194/acp-15-10149-2015, 2015.

Sun, Y., Zhuang, G., Tang, A. A., Wang, Y., and An, Z.: Chemical characteristics of $PM_{2.5}$ and PM_{10} in haze-fog episodes in Beijing, Environ. Sci. Technol., 40, 3148-3155, 10.1021/es051533g, 2006.

Tan, Z., Fuchs, H., Lu, K., Bohn, B., Broch, S., Dong, H., Gomm, S., Haeseler, R., He, L., Hofzumahaus, A., Holland, F., Li, X., Liu, Y., Lu, S., Rohrer, F., Shao, M., Wang, B., Wang, M., Wu, Y., Zeng, L., Zhang, Y., Wahner, A., and Zhang, Y.: Radical chemistry at a rural site (Wangdu) in the North China Plain: Observation and model calculations of OH, HO_2 and RO_2 radicals, Atmos. Chem. Phys. Discuss., 2016, 1-48, 10.5194/acp-2016-614, 2016.

Tham, Y., Yan, C., Xue, L., Zha, Q., Wang, X., and Wang, T.: Presence of high nitryl chloride in Asian coastal environment and its impact on atmospheric photochemistry, Chin. Sci. Bull., 59, 356-359, 10.1007/s11434-013-0063-y, 2014.

Thornton, J. A., Kercher, J. P., Riedel, T. P., Wagner, N. L., Cozic, J., Holloway, J. S., Dube, W. P., Wolfe, G. M., Quinn, P. K., Middlebrook, A. M., Alexander, B., and Brown, S. S.: A large atomic chlorine source inferred from mid-continental reactive nitrogen chemistry, Nature, 464, 271-274, 10.1038/nature08905, 2010.

Wagner, N. L., Riedel, T. P., Roberts, J. M., Thornton, J. A., Angevine, W. M., Williams, E. J., Lerner, B. M., Vlasenko, A., Li, S. M., Dube, W. P., Coffman, D. J., Bon, D. M., de Gouw, J. A., Kuster, W. C., Gilman, J. B., and Brown, S. S.: The sea breeze/land breeze circulation in Los Angeles and its influence on nitryl chloride production in this region, J. Geophys. Res.-Atmos., 117, D00V24, 10.1029/2012jd017810, 2012.

Wang, M., Zeng, L., Lu, S., Shao, M., Liu, X., Yu, X., Chen, W., Yuan, B., Zhang, Q., Hu, M., and Zhang, Z.: Development and validation of a cryogen-free automatic gas chromatograph system (GC-MS/FID) for online measurements of volatile organic compounds, Anal Methods, 6, 9424-9434, 10.1039/C4AY01855A, 2014.

Wang, T., Ding, A., Gao, J., and Wu, W. S.: Strong ozone production in urban plumes from Beijing, China, Geophys. Res. Lett., 33, L21806, 10.1029/2006GL027689, 2006.

Wang, T., Tham, Y. J., Xue, L. K., Li, Q. Y., Zha, Q. Z., Wang, Z., Poon, S. C. N., Dube, W. P., Blake, D. R., Louie, P. K. K., Luk, C. W. Y., Tsui, W., and Brown, S. S.: Observations of nitryl chloride and modeling its source and effect on ozone in the planetary boundary layer of southern China, J. Geophys. Res.-Atmos., 121, 2476-2489, 10.1002/2015JD024556, 2016.

Wang, X., Wang, T., Yan, C., Tham, Y. J., Xue, L., Xu, Z., and Zha, Q.: Large daytime signals of N_2O_5 and NO_3 inferred at 62 amu in a TD-CIMS: chemical interference or a real atmospheric phenomenon?, Atmos. Meas. Tech., 7, 1-12, 10.5194/amt-7-1-2014, 2014.

Wiedensohler, A., Birmili, W., Nowak, A., Sonntag, A., Weinhold, K., Merkel, M., Wehner, B., Tuch, T., Pfeifer, S., Fiebig, M., Fjäraa, A. M., Asmi, E., Sellegri, K., Depuy, R., Venzac, H., Villani, P., Laj, P., Aalto, P., Ogren, J. A., Swietlicki, E., Williams, P., Roldin, P., Quincey, P., Hüglin, C., Fierz-Schmidhauser, R., Gysel, M., Weingartner, E., Riccobono, F., Santos, S., Grüning, C., Faloon, K., Beddows, D., Harrison, R., Monahan, C., Jennings, S. G., O'Dowd, C. D., Marinoni, A., Horn, H.-G., Keck, L., Jiang, J., Scheckman, J., Mcmurry, P. H., Deng, Z., Zhao, C. S., Moerman, M., Henzing, B., De Leeuw, G., Löschau, G., and Bastian, S.: Mobility particle size spectrometers: harmonization of technical standards and data structure to facilitate high quality long-term observations of atmospheric particle number size distributions, Atmos. Meas. Tech., 5, 657- 685, 10.5194/amt-5-657-2012, 2012.

Xu, J., Ma, J. Z., Zhang, X. L., Xu, X. B., Xu, X. F., Lin, W. L., Wang, Y., Meng, W., and Ma, Z. Q.: Measurements of ozone and its precursors in Beijing during summertime: impact of urban plumes on ozone pollution in downwind rural areas, Atmos. Chem. Phys., 11, 12241-12252, 10.5194/acp-11-12241-2011, 2011.

Xue, L. K., Saunders, S. M., Wang, T., Gao, R., Wang, X. F., Zhang, Q. Z., and Wang, W. X.: Development of a chlorine chemistry module for the Master Chemical Mechanism, Geosci. Model Dev., 8, 3151-3162, 10.5194/gmd-8-3151-2015, 2015.

Yeung, M. C., Lee, B. P., Li, Y. J., and Chan, C. K.: Simultaneous HTDMA and HR-ToF-AMS measurements at the HKUST Supersite in Hong Kong in 2011, J. Geophys. Res.-Atmos., 119, 9864-9883, 10.1002/2013JD021146, 2014.

Young, C. J., Washenfelder, R. A., Edwards, P. M., Parrish, D. D., Gilman, J. B., Kuster, W. C., Mielke, L. H., Osthoff, H. D., Tsai, C., Pikelnaya, O., Stutz, J., Veres, P. R., Roberts, J. M., Griffith, S., Dusanter, S., Stevens, P. S., Flynn, J., Grossberg, N., Lefer, B., Holloway, J. S., Peischl, J., Ryerson, T. B., Atlas, E. L., Blake, D. R., and Brown, S. S.: Chlorine as a primary radical: evaluation of methods to understand its role in initiation of oxidative cycles, Atmos. Chem. Phys., 14, 3427-3440, 10.5194/acp-14-3427-2014, 2014.

Young, C. J., Washenfelder, R. A., Roberts, J. M., Mielke, L. H., Osthoff, H. D., Tsai, C., Pikelnaya, O., Stutz, J., Veres, P. R., Cochran, A. K., VandenBoer, T. C., Flynn, J., Grossberg, N., Haman, C. L., Lefer, B., Stark, H., Graus, M., de Gouw, J., Gilman, J. B., Kuster, W. C., and Brown, S. S.: Vertically resolved measurements of nighttime radical reservoirs in Los Angeles and their contribution to the urban radical budget, Environ. Sci. Technol., 46, 10965-10973, 10.1021/es302206a, 2012.

Yuan, B., Chen, W. T., Shao, M., Wang, M., Lu, S. H., Wang, B., Liu, Y., Chang, C. C., and Wang, B. G.: Measurements of ambient hydrocarbons and carbonyls in the Pearl River Delta (PRD), China, Atmos. Res., 116, 93-104, 10.1016/j.atmosres.2012.03.006, 2012.

Yuan, B., Liu, Y., Shao, M., Lu, S. H., and Streets, D. G.: Biomass burning contributions to ambient VOCs species at a receptor site in the Pearl River Delta (PRD), China, Environ. Sci. Technol., 44, 4577-4582, 10.1021/es1003389, 2010.

Zhang, L., Wang, S., Meng, Y., and Hao, J.: Influence of mercury and chlorine content of coal on mercury emissions from coal-fired power plants in China, Environ. Sci. Technol., 46, 6385-6392, 10.1021/es300286n, 2012.

Zhang, Q., Yuan, B., Shao, M., Wang, X., Lu, S., Lu, K., Wang, M., Chen, L., Chang, C. C., and Liu, S. C.: Variations of ground-level O_3 and its precursors in Beijing in summertime between 2005 and 2011, Atmos. Chem. Phys., 14, 6089-6101, 10.5194/acp-14-6089-2014, 2014.

Zhao, Y., Wang, S. X., Duan, L., Lei, Y., Cao, P. F., and Hao, J. M.: Primary air pollutant emissions of coal-fired power plants in China: Current status and future prediction, Atmos. Environ., 42, 8442-8452, 10.1016/j.atmosenv.2008.08.021, 2008.

Table 1. Measurement method for trace gases and aerosols.

Species	Measurement Techniques	Detection Limits	Uncertainty	Time resolution
$ClNO_2$, N_2O_5	CIMS	6-7 pptv	25%	1 min
O_3	UV photometry	0.5 ppbv	5%	1 min
NO	Chemiluminescence	0.06 ppbv	20%	3 min
NO_2	Photolytical converter & Chemiluminescence	0.3 ppbv	20%	1 min
NO_y	MoO catalytic converter & Chemiluminescence	<0.1ppbv	5%	1 min
CH_4	CRDs	0.1 ppmv	<5%	1 min
SO_2	Pulsed-UV fluorescence	0.1 ppbv	5%	1 min
CO	IR photometry	4 ppbv	5%	1 min
HONO	LOPAP	7 pptv	20%	0.5 min
HCl	GAC-IC	59 pptv	10%	30 min
NMHCs	GC-FID/MS	20 - 300 pptv	15-20%	60 min
OVOCs	PTR-MS	10 - 50 pptv	15%	5 min
Formaldehyde	Hantzsch (wet chemical fluorimetric)	25 pptv	5%	1 min
$PM_{2.5}$	TEOM	2 $\mu g/m^3$	10%	1 min
Aerosol ionic compositions	GAC-IC	0.01-0.16 $\mu g/m^3$	10%	30 min

Table 2. Correlations of chloride with power plant and biomass burning indicators (from 20:00-09:30 LT).

Duration (20:00-09:30)	[Cl⁻] Mean (μg m^{-3})	Power plant indicator (SO$_2$) Mean (ppbv)	Slope	Correlation (*r*)	Biomass burning indicator (CH$_3$CN) Mean (ppbv)	Slope	Correlation (*r*)
20-21 June	1.450	5.74	0.092	0.858	0.35	2.20	0.330
21-22 June	2.792	3.87	0.267	0.963	*n/a*	*n/a*	*n/a*
23-24 June	1.729	5.65	0.234	0.946	0.43	0.10	0.003
24-25 June	0.760	4.88	0.235	0.852	0.39	36.96	0.547
25-26 June	1.988	2.79	0.281	0.833	0.56	11.27	0.893
27-28 June	0.335	6.67	0.008	0.213	0.39	-1.33	0.577
28-29 June	0.915	7.44	0.083	0.831	0.55	2.77	0.830
29-30 June	1.429	22.67	0.048	0.719	0.48	4.96	0.442
30 June – 1 July	1.283	10.43	0.094	0.781	0.45	6.01	0.268
01-02 July	0.762	2.53	0.089	0.630	0.32	4.76	0.448
02-03 July	2.187	3.84	0.195	0.762	0.43	10.68	0.548
03-04 July	2.636	3.69	0.314	0.613	0.39	12.76	0.566
04-05 July	2.158	2.55	0.365	0.922	0.35	30.09	0.924
05-06 July	2.857	7.29	0.112	0.776	0.44	12.86	0.763
06-07 July	1.720	6.04	0.113	0.853	0.46	9.84	0.502
07-08 July	1.939	8.70	0.084	0.607	0.49	2.14	0.157
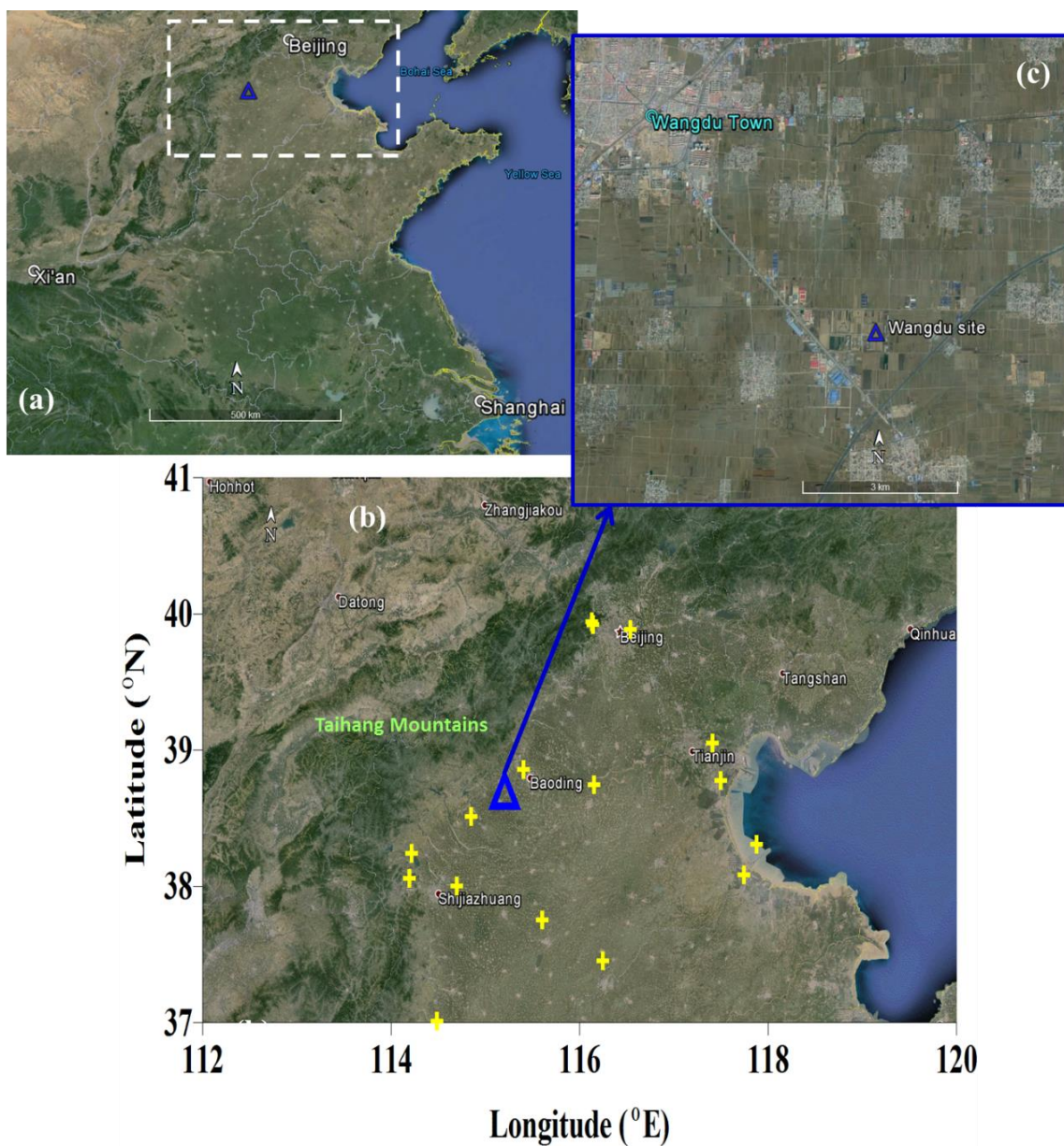
Figure 1. Google map showing a) the location of northern China (white dash-box) and Wangdu site (blue triangle), b) an expanded view of northern China plain with the topography, major cities and the locations of major coal-fired power plants (yellow cross) in the region, c) nearby environment of Wangdu site.
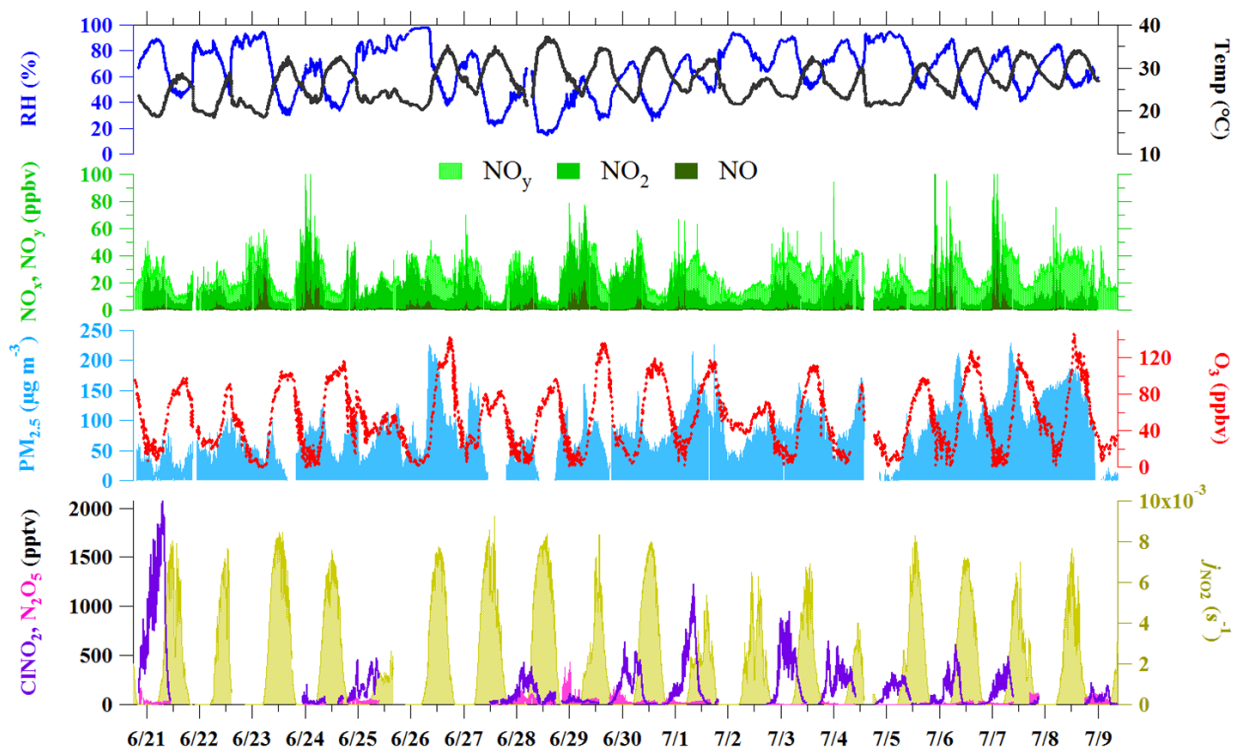
Figure 2. Time series of ClNO₂, N₂O₅ together with related species and meteorological data. Data are at 1-minute time resolution, except for NOₓ data which are 5-minute averages.
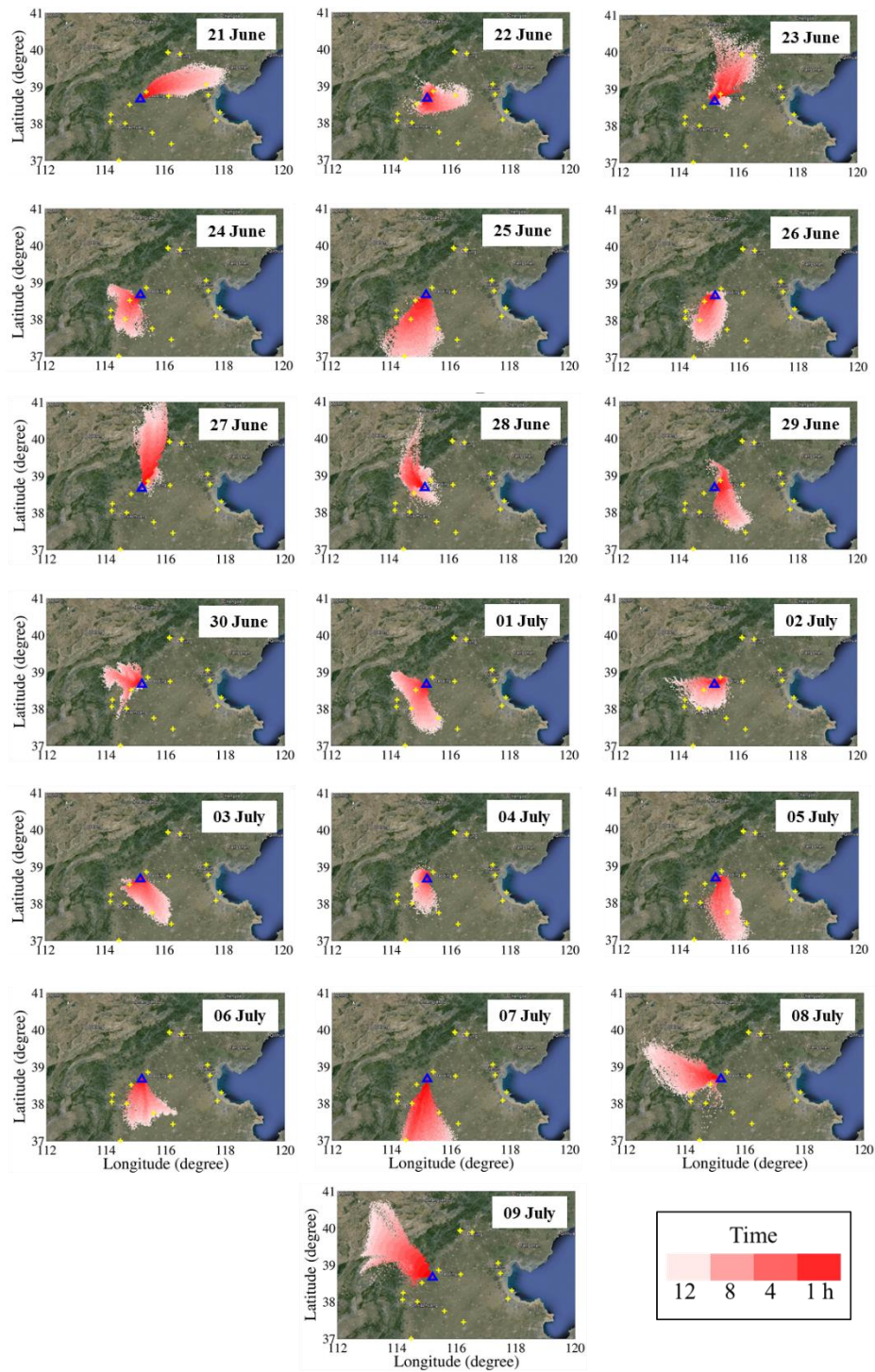
Figure 3. 12-hour history of air masses arriving at the measurement site at 08:00. Yellow cross represents major coal-fired power plants in the region.
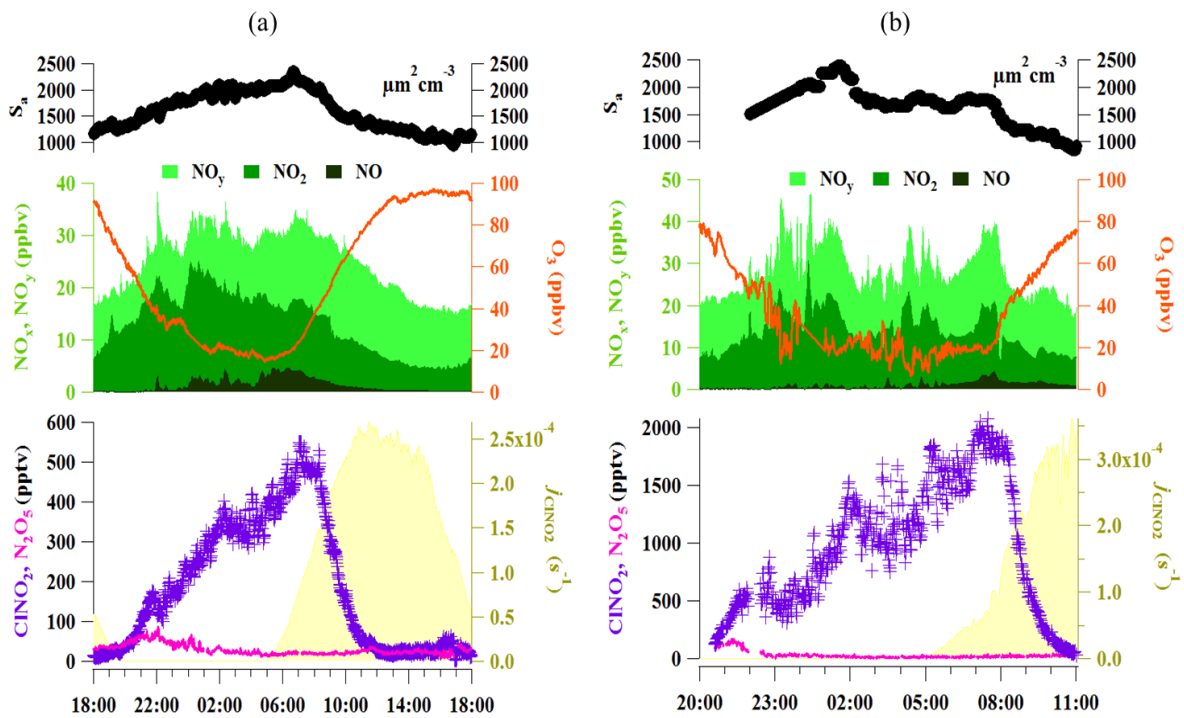
Figure 4. Diurnal variations of ClNO₂, N₂O₅, NOₓ, NOᵧ, O₃ and particle surface area for a) campaign average (from 20 June to 9 July 2014 when ClNO₂ data is available) and b) the highest ClNO₂ case on 20-21 June 2014 (the megacity case).
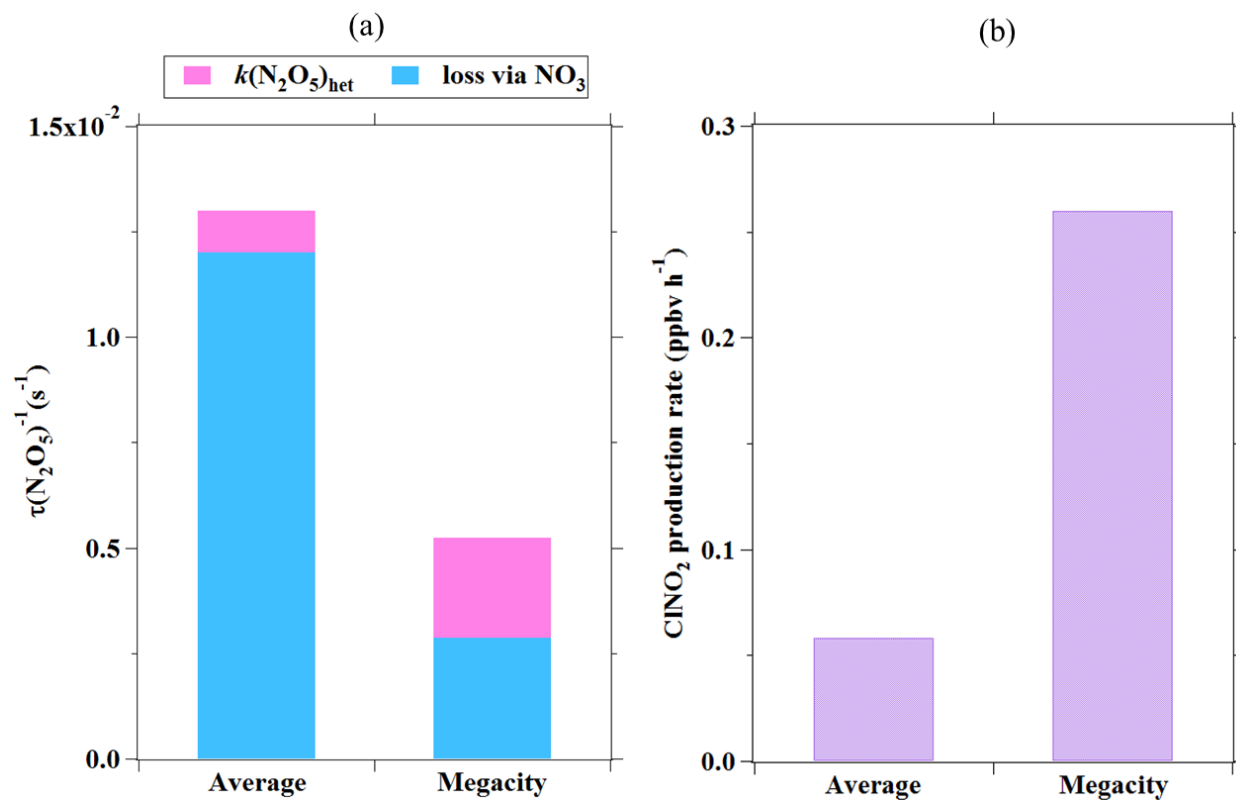
Figure 5. a) Fractions of N₂O₅ loss rate coefficient through NO₃, homogenous and heterogeneous reaction of N₂O₅ for campaign average and the megacity case; b) the calculated ClNO₂ production rate for campaign average and the megacity case.
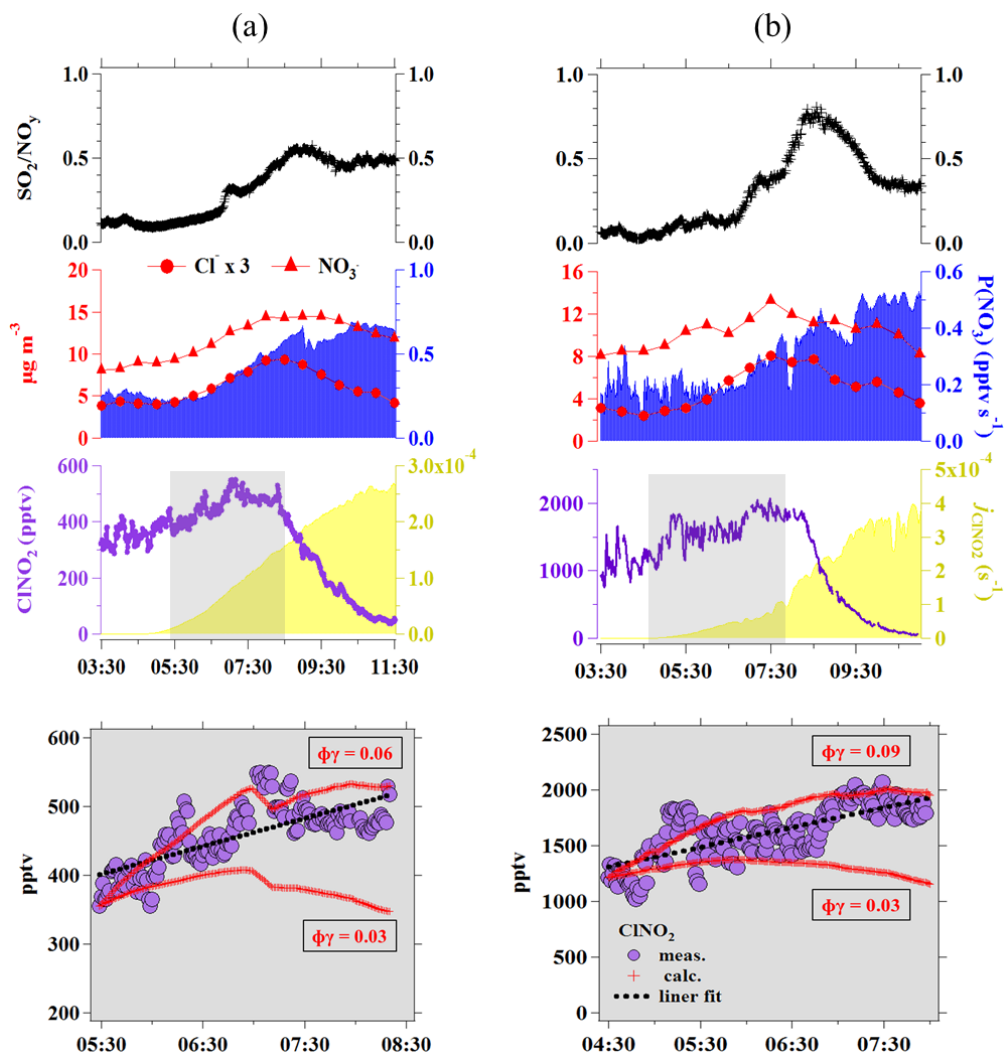
Figure 6. Expanded view of the sustained morning ClNO₂ peaks for a) campaign average and b) the megacity case. The upper panel shows some relevant chemical information including SO₂/NOy, Cl⁻, NO₃⁻, and P(NO₃). The increase of ClNO₂ in the shaded area (light grey) are compared to the calculated in-situ production of ClNO₂ (lower panel).
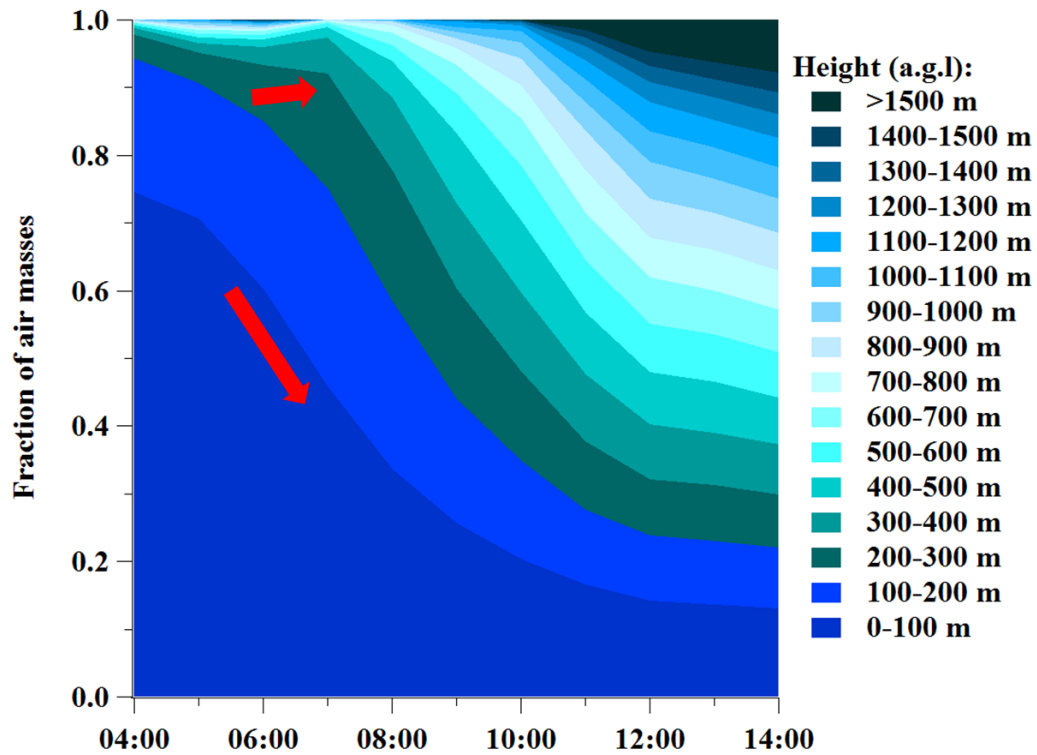
Figure 7. Fractions of air masses arriving at the measurement site at different time of the day (average condition). It is noted that these fractions were derived from the 1 h backward-in-time HYSPLIT simulation results. Red arrows show the decreased contribution of lower layer (<200m) and increased contribution from upper layer (>200m) air masses shortly after sunrise.
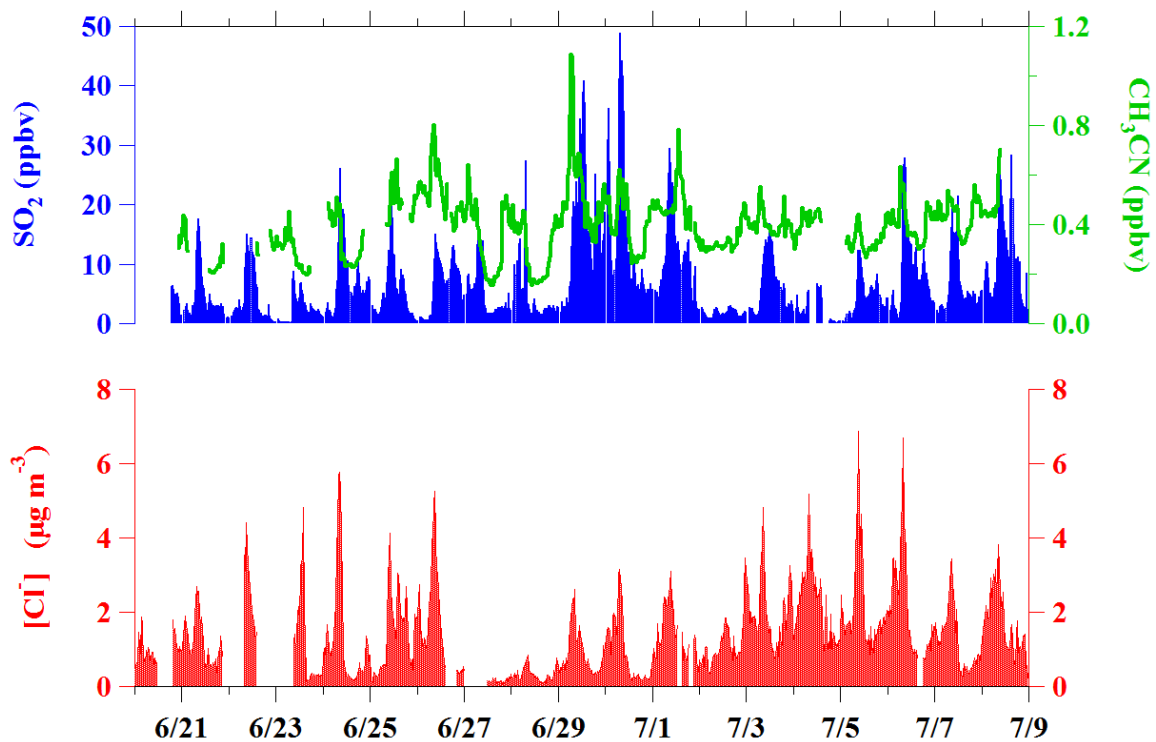
Figure 8. Time series of Cl⁻ aerosol, SO₂ (a coal-fired power plant indicator) and CH₃CN (a biomass burning indicator) from 20 June to 9 July 2014.
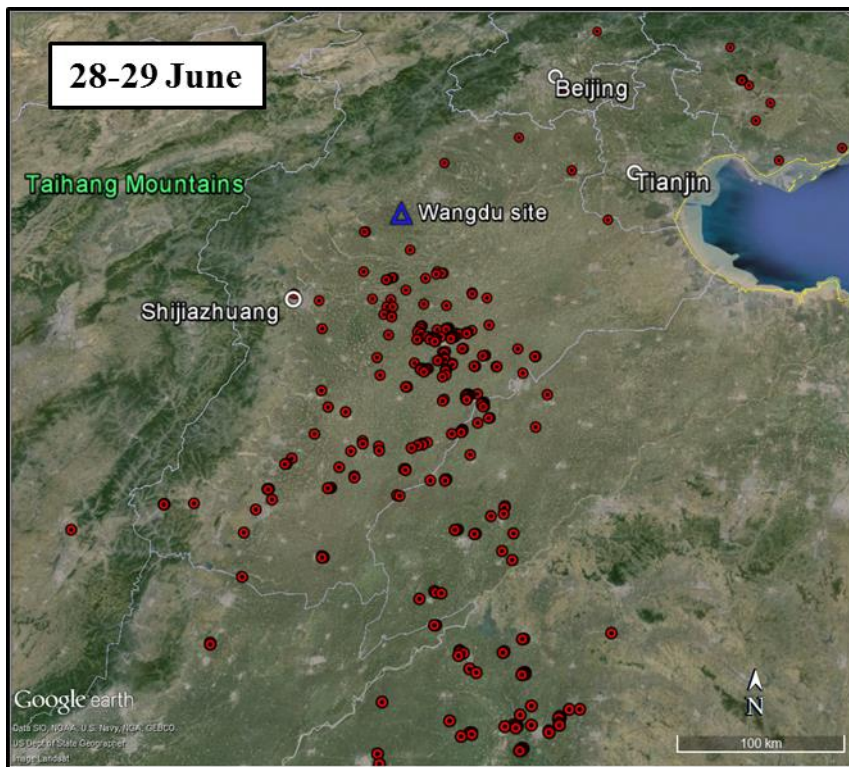
Figure 9. Biomass burning activities from the active fire hotspots data (red dots) on 28-29 June 2014 (Data available at https://earthdata.nasa.gov/firms).
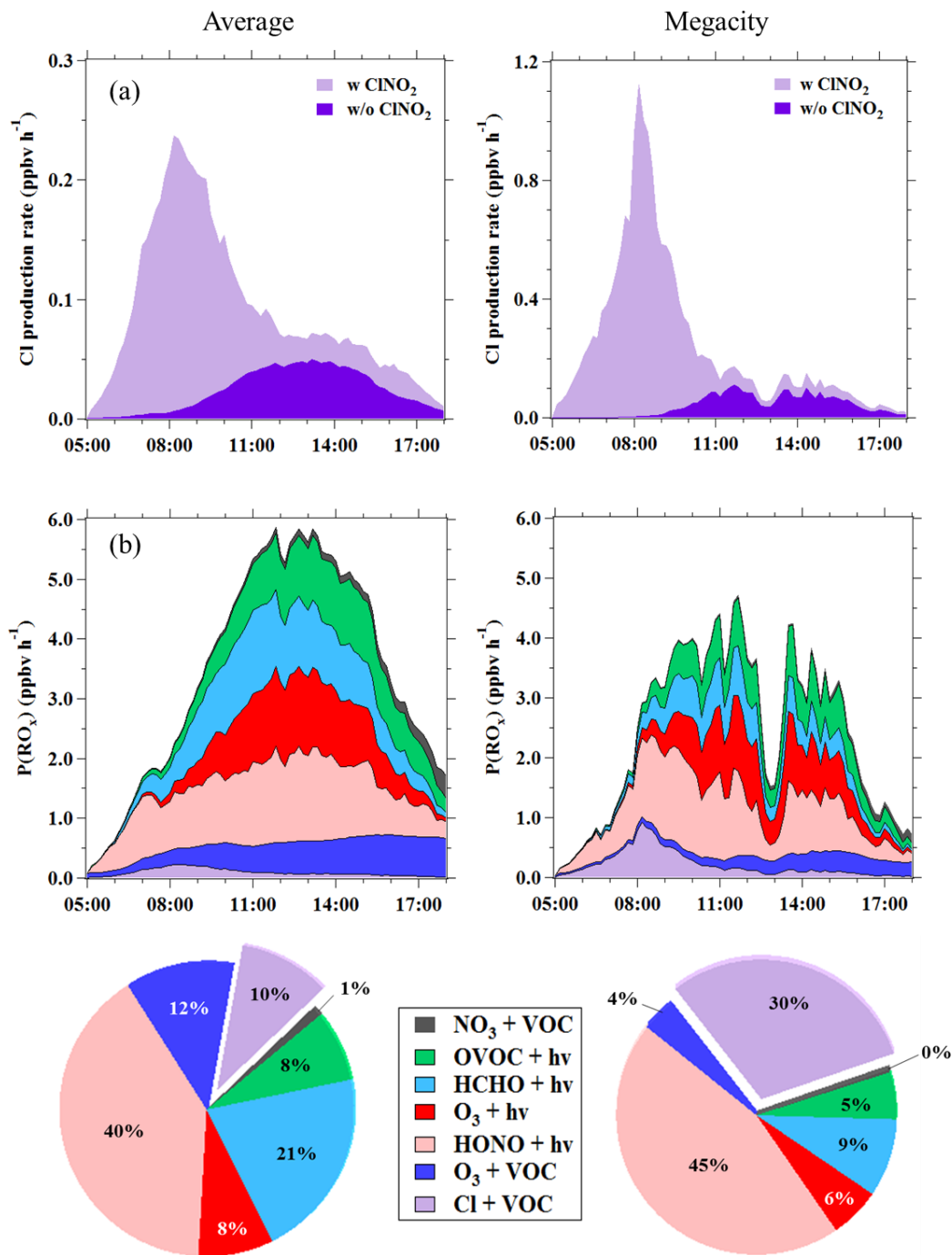
Figure 10. a) Cl production rates with ClNO₂ and without ClNO₂ input; b) primary ROₓ radical production rates from different sources at Wangdu in the daytime. Pie charts represent the contributions of ClNO₂ to the primary ROₓ radical production in the morning time (average value for 08:00-08:30).
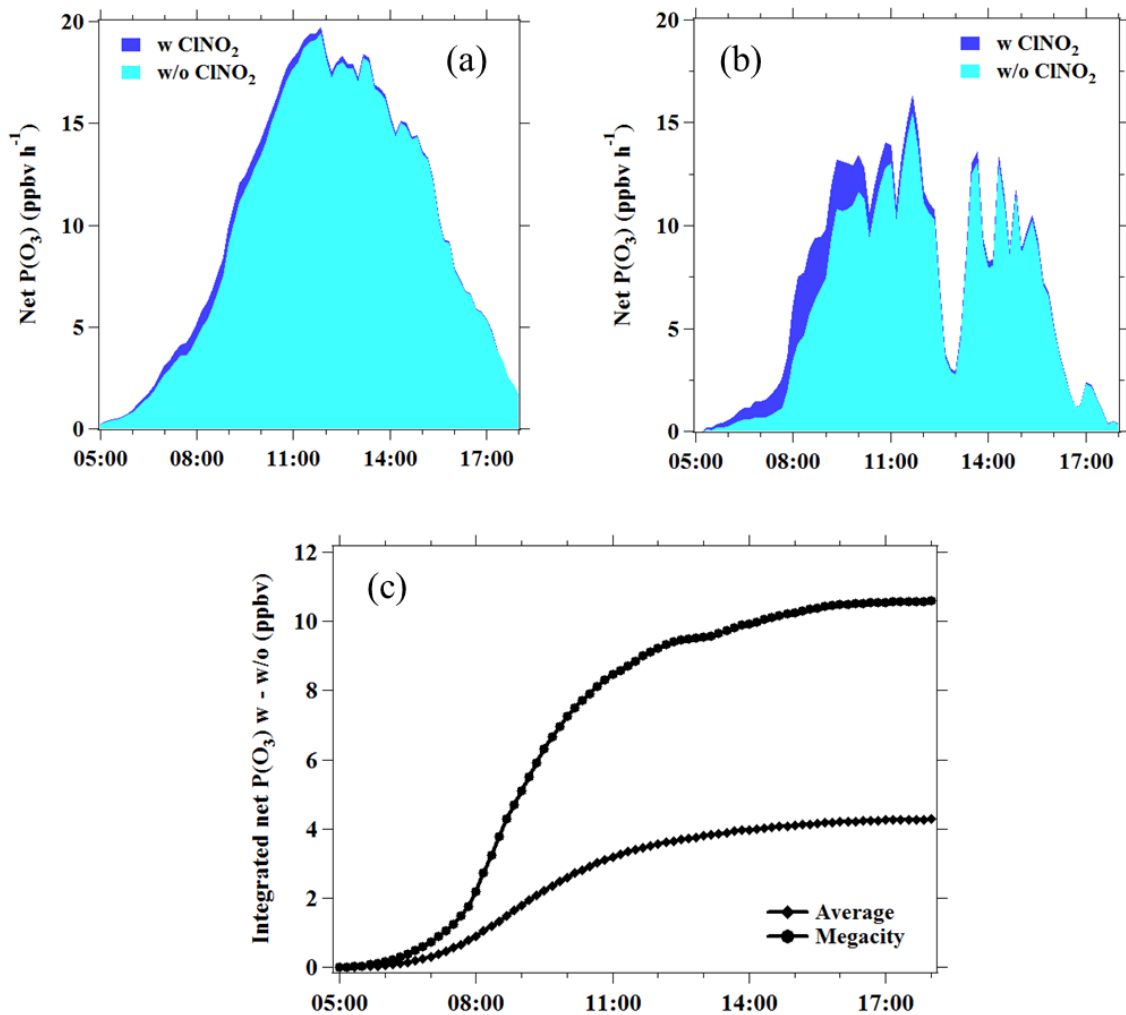
Figure 11. Net ozone production rates for a) average, b) the megacity case and c) the difference in integrated net ozone production rate between the simulation with and without the ClNO₂ input.